DESIGN OF A MODIFIED CLASS EF_2 INVERTER FOR ELECTRIC VEHICLE CHARGING THROUGH WIRELESS POWER TRANSFER

MOHAMMAD KAMAR UDDIN

FACULTY OF ENGINEERING
UNIVERSITY OF MALAYA
KUALA LUMPUR

2017

DESIGN OF A MODIFIED CLASS EF_2 INVERTER FOR ELECTRIC VEHICLE CHARGING THROUGH WIRELESS POWER TRANSFER

MOHAMMAD KAMAR UDDIN

DISSERTATION SUBMITTED IN FULFILMENT OF THE REQUIREMENTS FOR THE DEGREE OF MASTER OF ENGINEERING SCIENCE

FACULTY OF ENGINEERING
UNIVERSITY OF MALAYA
KUALA LUMPUR

2017

UNIVERSITY OF MALAYA

ORIGINAL LITERARY WORK DECLARATION

Name of Candidate: Mohammad Kamar Uddin

Matric No: KGA140036

Name of Degree: Master of Engineering Science

Title of Dissertation ("this Work"):

DESIGN OF A MODIFIED CLASS EF_2 INVERTER FOR ELECTRIC VEHICLE CHARGING THROUGH WIRELESS POWER TRANSFER

Field of Study: Power Electronics

I do solemnly and sincerely declare that:

(1) I am the sole author/writer of this Work;
(2) This Work is original;
(3) Any use of any work in which copyright exists was done by way of fair dealing and for permitted purposes and any excerpt or extract from, or reference to or reproduction of any copyright work has been disclosed expressly and sufficiently and the title of the Work and its authorship have been acknowledged in this Work;
(4) I do not have any actual knowledge nor do I ought reasonably to know that the making of this work constitutes an infringement of any copyright work;
(5) I hereby assign all and every rights in the copyright to this Work to the University of Malaya ("UM"), who henceforth shall be owner of the copyright in this Work and that any reproduction or use in any form or by any means whatsoever is prohibited without the written consent of UM having been first had and obtained;
(6) I am fully aware that if in the course of making this Work I have infringed any copyright whether intentionally or otherwise, I may be subject to legal action or any other action as may be determined by UM.

Candidate's Signature Date:

Subscribed and solemnly declared before,

Witness's Signature Date:

Name:

Designation:

ABSTRACT

Wireless power transfer (WPT) also referred as inductive power transfer (IPT) has the huge potentiality to revolutionize our way of electricity usage. This technology has found many applications like charging autonomous mobile devices like mobile phone, autonomous guided vehicles as well as industrial process system, biomedical implant and electric vehicle charging. These applications involve power transfer from small level (1 W) to a high level (10-20 kW) with a large air gap (5-50 cm).

A complete IPT system usually consists of several stages: grid or utility AC to DC conversion, the rectified DC to high-frequency AC conversion, primary compensation, WPT coils (loosely coupled transformer), secondary compensation and AC/DC/DC conversion. Among these, high-frequency DC/AC conversion plays a vital role to transfer high power, to increase gap distance and overall system efficiency. The focus of this research is to design and evaluate a single switch high-frequency resonant inverter for WPT vehicle charging application capable of transferring power up to 3 kW. Single switch resonant inverter topologies are potential for WPT application. The capability of operating with high frequency and high power, ease of control circuit design and compactness are some of the main features of these types of inverters.

In this research, a modified single switch resonant inverter termed as class EF_2 will be designed and evaluated for standard vehicle charging system frequency (85-100 kHz). This is the major contribution of this research. A detail mathematical model is developed which includes the significant parasitic elements of the overall system on this frequency range. Furthermore, a series tuned passive resonant circuit is used for second harmonic termination which reduces the switching stress significantly from all other single switch topology. The placement of this passive resonant circuit for reducing switch stress and input DC-feed inductance characteristic is also analysed. Power transfer capability,

switch stress and reactive power circulation during misalignment and coupling variation condition have been evaluated experimentally with constant frequency and with a frequency variation of 5-10%. Finally, inverter efficiency on perfectly align to 30% misalignment and variation of output voltage with load variation will be evaluated.

ABSTRAK

Pemindahan tenaga tanpa wayar (WPT) juga dirujuk sebagai pemindahan kuasa induktif (IPT) mempunyai potensi yang besar untuk merevolusikan cara penggunaan elektrik. Teknologi ini telah menemui banyak aplikasi seperti mengenakan peranti mudah alih autonomi seperti telefon bimbit, kenderaan dipandu autonomi serta sistem proses industri, implan bioperubatan dan kenderaan elektrik mengecas. Aplikasi ini melibatkan pemindahan kuasa dari peringkat kecil (1 W) ke tahap yang tinggi (10-20 kW) dengan ruang udara yang besar (5-50 cm).

Sistem IPT lengkap biasanya terdiri daripada beberapa peringkat: grid atau AC utiliti untuk DC penukaran, yang diperbetulkan DC untuk frekuensi tinggi AC penukaran, pampasan utama, gegelung WPT (longgar ditambah pengubah), pampasan menengah dan AC / DC / DC penukaran. Antaranya, penurakan frekuensi tinggi DC / AC memainkan peranan yang penting untuk memindahkan kuasa tinggi, untuk meningkatkan jarak jurang dan kecekapan sistem secara keseluruhan. Fokus kajian ini adalah untuk mereka bentuk dan menilai satu suis frekuensi tinggi inverter salunan untuk kenderaan WPT mengecas permohonan yang boleh memindahkan kuasa sehingga 3 kW.

Topologi suis tunggal penyongsang salunan berpotensi untuk aplikasi WPT. Keupayaan beroperasi dengan frekuensi tinggi dan berkuasa tinggi, memudahkan reka bentuk litar kawalan dan kompak adalah beberapa ciri-ciri utama jenis penyongsang. Dalam kajian ini, penyongsang salunan diubahsuai suis tunggal disebut sebagai kelas EF_2 direka dan dinilai untuk standard frekuensi sistem kenderaan pengecasan (85-100 kHz). Ini adalah sumbangan utama kajian ini. Suatu model matematik terperinci dibangunkan yang merangkumi unsur-unsur parasit besar daripada sistem keseluruhan pada julat frekuensi ini. Tambahan pula, siri yang ditala litar salunan pasif digunakan untuk penamatan harmonik kedua yang mengurangkan tekanan pensuisan dengan ketara daripada semua suis lain topologi tunggal.

Penempatan litar salunan pasif ini untuk mengurangkan tekanan suis dan masukan DC, kearuhan ciri juga dianalisis. Keupayaan pemindahan kuasa, suis tekanan dan peredaran kuasa reaktif semasa juling dan keadaan gandingan variasi telah dinilai secara eksperimen dengan kekerapan yang tetap dan dengan variasi kekerapan 5-10%. Akhirnya, kecekapan penyongsang sempurna menyelaraskan 20% jajaran dan perubahan voltan output dengan perubahan beban akan dinilai.

ACKNOWLEDGEMENTS

First, I am thankful to the Almighty ALLAH for enabling me to complete this challenging task.

I would like to thank my supervisor Professor Dr. Saad Mekhilef for his supervision and experience guidance. His continuous financial support and encouragement throughout my candidature gave me more confidence in my work and abilities and led me to overcome all the difficulties during my study. It is my valued opportunity to learn the rigorous attitude towards study and research from him. I would also like to thank Prof. Dr. Mutsuo Nakaoka and Dr. Gobbi Ramasamy for their valuable discussions, cooperation and support.

This journey would not have been pleasant without my friends and fellow members from PEARL lab especially S M Showybul Islam Shakib, Md Morshed Alam, Toffael Ahmed, Abdul Mannan Dadu, Md Didarul Islam, Md Haidar Islam, Rasedul Hasan and Kafeel Ahmed Kalwar.

My deepest gratitude belongs to my parents Mr. Mohammad Zaynal Abddin and Ms. Rehena Begum for their countless prayers, love, sacrifice for my study.

I owe every part of this work to my wife Chowdhury Mahbuba Arzima who has sacrificed a lot during my study.

TABLE OF CONTENTS

LIST OF FIGURES

LIST OF TABLES

LIST OF SYMBOLS AND ABBREVIATIONS

WPT	:	Wireless Power Transfer
IPT	:	Inductive Power Transfer
HF	:	High Frequency
EV	:	Electric Vehicle
ZVS	:	Zero Voltage Switching
CPT	:	Capacitive Power Transfer
MRC	:	Magnetic Resonance Coupling
PHEV	:	Plug-in Hybrid Electric Vehicle
SAE	:	Society of Automotive Engineers
ZCS	:	Zero Current Switching
FHA	:	First Harmonic Approximation
ORNL	:	Oak Ridge National Laboratory
ZdVS	:	Zero Slope Switching
ZDS	:	Zero Derivative Switching
BEV	:	Battery Electric Vehicle
SOA	:	Safe Operating Area

CHAPTER 1: INTRODUCTION

1.1 Research Background

Electrical energy has always been transferred by utilising conductors or otherwise known as wires. Electric current can flow in a conductor if an electric potential difference is applied across the conductor, consequently, electric power can be transferred from a source such as a generator or a battery to a load. The usage of cables and wires is the preferred choice to connect a source to a load. It is a simple and efficient method to transfer electrical energy and it is suitable for most of the today's applications since the loads, whether in industry or in our homes, are stationary and motionless. However, relying on a cable connected to a power outlet to obtain energy may not be the only practical solution anymore. New applications are being developed and introduced that are mobile and require a continuous or semi-continuous power supply. Therefore, having a direct cable connection may limit their freedom of movement and in some cases, may not be a safe option. For example, the research and development in hybrid and electric vehicles are on the rise due to the increase in oil prices and to environmental concerns. These vehicles have an onboard battery that can provide power partially or entirely for the entire trip duration. Although a direct cable connection to a power outlet is suitable to a certain degree to provide power and recharge the batteries, more options will be available if that power was supplied wirelessly without cables and contacts. The vehicle, for example, could be powered 'on the go' while it is moving. The risk of electric shock and sparks is highly reduced since no contacts are used, maintenance requirements are also reduced since there is no wear and tear involved in the powering and charging process.

Development of power semiconductor switching devices and innovative power conversion techniques have made possible to transfer electrical energy across a large air gap. This is referred as wireless power transfer (WPT) or more conveniently as inductive

power transfer (IPT). WPT or IPT may seem as an alternative method to power today's and the future's applications. The key point involved in this novel technique is the power conversion from a low-frequency system such as a DC or 50/60Hz mains power supply to a much higher frequency system with a frequency of about 10-100 kHz (Hu, 2001). This power conversion makes power flow across an air gap feasible in practice. Thus, power electronics converters are enabling technology for IPT system particularly high-frequency inverter which creates high-frequency AC. However, many design challenges, technological obstacles, and commercialization prospect need to be addressed and overcome for these power electronics converters and inverters.

1.2 Research Motivation

IPT technology has certainly matured to a level where applications and products can now be developed and commercialised. In fact, it is one of the fastest growing technologies that evolved from a concept to technology demonstration, and finally to product development. The number publications in IPT system are increasing exponentially, with many international conferences and exhibitions entirely dedicated for wireless power transfer.

Recent research in IPT technology aiming towards low-level power transfers to high-level power transfer. Very low power level (less than1 W) applications tend to be biomedical implantable devices or sensors. These applications require a relatively high-frequency operation (usually MHz range), low efficiency and a short gap distance. Applications which are of 1 W to less than 1 kW range typically consumer electronics, e.g. cell phones, TVs, and lighting. Some niche biomedical applications may also get significant power but less than 1 kW. In this range, the efficiency, frequency, and gap distance vary greatly, but short distance high-frequency IPT appears to have acceptable efficiency and cost as it is already commercialized. Longer distance low-power IPT

systems are still in development. Deployed medium-to high-power level (more than 1 kW) applications include automotive assembly lines, clean factories, and general industrial automation applications. Research is ongoing into electric vehicle charging with interest growing steadily. These types of applications usually have a higher gap distance (e.g. >10 cm) and the operational frequency is generally low due to power electronics limitations.

Despite its maturity, IPT technology is still yet to unleash its full potential. The applications and products that are being developed still do not demonstrate what IPT technology can achieve. It is about time to take IPT technology to the next level by introducing applications and concepts that can never be realised without it. Concepts such as dynamic vehicle-to-vehicle charging, in-flight charging for electric airborne vehicles and wireless power for remote-controlled planetary exploration robots are all examples of what IPT technology can potentially achieve. In this research, IPT electric vehicle (EV) charging will be focused. Figure 1.1 shows the current global EV sales and market share. It shows that EV sale is increased significantly since 2012. It also depicts that Norway, Netherlands and US has considerable market share on EV market.

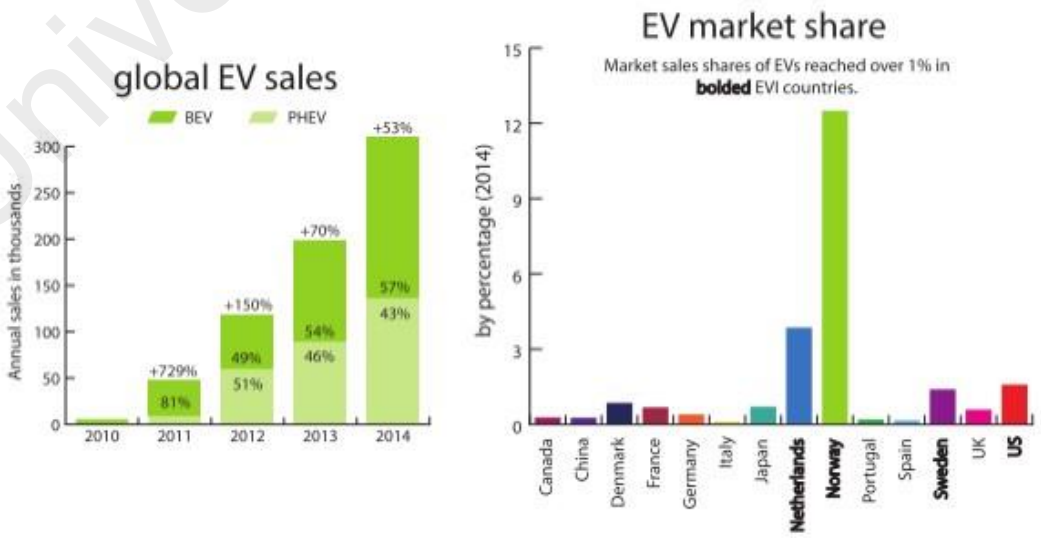

Figure 1.1: Global EV Sales and Market Share Outlook (Bosshard, 2015)

1.3 Problem Statement

A typical IPT (WPT) system utilizes a primary coil to generate a time-varying magnetic fields which travel over a gap distance to energizes a secondary coil for transferring power. Resonance phenomena are used in IPT system to transfer power efficiently across the large air gap. This secondary induced voltage then conditioned to supply a specific load or charge battery of an EV. A higher resonance frequency is required to enhance the range and power transfer capability (Aldhaher, Luk, & Whidborne, 2014b). Thus, a powerful primary side inverter capable of operating at the higher frequency and capable of delivering high power is required for an efficient IPT system.

High frequency (HF) and high-power level power electronic inverter design, especially for WPT systems, are challenging because displacement and gating loss of power semiconductor devices and parasitic of various circuit components play very active roles during high frequency operation (Perreault et al., 2009). Switching losses, large *dv/dt* and *di/dt* during switching operation and hence excessive EMI are some of the major limitations for existing hard switched converters and PWM inverters (Ching & Chan, 2008). Resonant inverters are well suited to overcome these limitations of conventional inverters and can provide high frequency operation while maintaining high efficiency. However, complexities of the IPT system such as primary compensation circuit, primary-secondary coil misalignment, coupling and load variation add more challenges in the resonant inverter design process.

In the latest literature, different types of IPT primary side resonant inverter topologies have been described depending on the application area. Applications which require power level 1 kW and higher dominantly use bridge configuration with series LC resonant (SLC)

and series-parallel resonant (LCL) compensation topologies (Esteban, Sid-Ahmed, & Kar, 2015). In (Qu, Jing, Han, Wong, & Tse, 2017), authors proposed various higher-order compensation topologies for IPT system. However, a single switch class E resonant inverter and its variants can also meet the requirement of IPT systems because of their ability to deliver medium power (1-5 kW) at higher switching frequency (Aldhaher, Kkelis, Yates, & Mitcheson, 2015; Aldhaher, Luk, et al., 2014b; Jungwon, Tsukiyama, Tsuruda, & Rivas, 2015). Single switch resonant inverters are attractive for simplicity, low component count and simple gate driver circuitry and timing control. They make the system more compact and robust. Although these types of inverters have many attractive features, but they are subjected to degraded performance in case of coupling and load variation in IPT system. To overcome these limitations, electronic tuning methods have been proposed in the literature (Aldhaher, Luk, & Whidborne, 2014a; Aldhaher, Luk, et al., 2014b). The misalignment problem will be further reduced using movable primary coil mechanism or using automatic parking assistance system. As now these types of mechatronics system are easier and cheaper to design, so misalignment problem for single switch type inverters will not be a serious problem.

Another major problem with these types of inverters is the large switch stress (3.5 times input DC). In IPT system, significant variation of reflected impedance seen by the inverter occurs during gap change between primary and secondary coil, misalignment and variable load conditions. This would make the switching stress much worse which in turn may cause permanent damage of the semiconductor switch. To overcome high switching stress and improve the efficiency of class E inverter, a passive resonant network can be added in parallel with load network. This type modified class E inverter is referred as Class EF/EF_n inverter (Aldhaher, Yates, & Mitcheson, 2015; Kaczmarczyk, 2006; Kee, Aoki, Hajimiri, & Rutledge, 2003; Mediano & Sokal, 2013). These types of inverters

reduce the voltage stress to 2.5 times which is significantly less than class E inverter. Performance and power output capability of these inverters are also higher.

However, by placing the passive resonant circuit between DC-feed inductor and semiconductor switch the voltage stress could be further reduced (almost 2 times of input DC). This type of inverters is referred as Class Φ inverter in the literature (Phinney, Perreault, & Lang, 2007; Rivas, Han, Leitermann, Sagneri, & Perreault, 2008). Both types of inverters demonstrate good potentiality in various IPT applications. However, to the best of author knowledge till date, detail design of these types of inverters has been discussed for 800 kHz – 13.6 MHz frequency range IPT system. These frequency ranges are not well suited for EV charging application. According to SAE regulation (expected to be published by 2017) for wireless EV charging 85 – 100 kHz frequency range will be used. Furthermore, the whole WPT system has been designed around the inverter which is also a drawback while designing a practical IPT system. Because primary and secondary coil values were calculated to obtain maximum efficiency and reduce switching stress of the inverter. So, it is important to evaluate the performance of these types of inverters in low frequency (up to 100 kHz) region with practical coil parameter to observe the universality and usability of these types of inverter topologies in IPT EV charging application.

In this research, a modified class EF_2 voltage-fed multi-resonant single switch inverter topology has been proposed for IPT applications. A constant frequency of 100 kHz has been chosen in this research. Based on predetermined coil parameters, the rest of the components of the inverter will be calculated. A practical tuning method for a various component of the inverter will be provided. Afterwards, overall IPT system will be analysed for transfer efficiency and zero voltage switching (ZVS) of the inverter. The proposed inverter has all the advantages of class E inverter. At the same time, it

overcomes some of the critical drawbacks of class E inverter which degrades the inverter performance while used with IPT system. Switch stress variation due to change of coupling, coil misalignment and load variation are most important among those drawbacks. Thus, these have been discussed in this research.

1.4 Research Objectives

1. Design and analysis of a modified class EF_2 inverter for IPT EV charging system with fixed IPT coil parameters.
2. To build a 150W modified class EF_2 prototype to verify the theoretical design for a pre-built IPT coil.
3. To compare the performance of the prototype with existing class E and class EF_2 inverter.

1.5 Dissertation Outline

This report is divided into five chapters including this introductory chapter. The remaining chapters are organized as follows:

Chapter 2 presents a review of the current literature in commonly used WPT methods, various stages of IPT system, compensation topologies, primary side inverter topologies, critical assessment of these topologies and proposed topology.

Chapter 3 describes the design procedure of modified class EF_2 inverter topology and some relevant discussion of class E inverter.

Chapter 4 will provide the simulation result, prototype description and experimental result.

Chapter 5 will present discussion, conclusion and future work.

CHAPTER 2: LITERATURE REVIEW

2.1 Introduction

Resonant inductive link IPT system finds application in factory automation, for lighting application, for instrumentation and electronic system, biomedical implant and lots of other application where its unique features can be exploited (Esteban et al., 2015; Jiejian & Ludois, 2015). Recently, IPT technology has gained attention to the automotive industries. This is due to the public awareness of environmental impact of greenhouse gas and development of modern lithium-ion batteries. Furthermore, total ownership cost of EV over the lifetime is lower than that of traditional vehicles despite higher initial purchase cost (Bosshard, 2015). Hence, EV sales rapidly increasing in the market of the developed world (Bosshard, 2015). Thus, various industrial giants (GM, BMW, Mitsubishi, and Toyota) in the vehicle industry have increased their research efforts to develop electric vehicles (EVs). This recent trend of EV developing also presents a vital issue of their charging method.

In this chapter, first, an overview of various wireless EV charging methods will be discussed. The opportunity of IPT system for vehicle charging and theory of high frequency inverter design will be discussed afterward. Various stages of IPT EV charging system will be described with the focus of compensation topologies and primary side inverter. The importance of primary side inverter topology in IPT system and commonly used inverters will be described. Finally, advantages of resonant inverters for IPT system, the single switch resonant inverter in IPT system and their research gap will be discussed to relate with a research focus.

2.2 Wireless Power Transfer Method for EV charging

A typical wireless EV charging schematic has been shown in figure 2.1. Different WPT methods have been employed so far for high power electric vehicle (EV) charging.

Nearly all of these methods rely on near-field coupling mechanism and can be divided into two methods: magnetic induction or inductive power transfer (IPT) and electrostatic induction or capacitive power transfer (CPT) (Jiejian & Ludois, 2015). Another popular WPT method known as microwave power transfer (MPT) which is commonly used for information transfer is also being investigated for vehicle charging. However, this method has not gained much research attention till date. Another recently introduced WPT method called magnetic resonance coupling (MRC) is also gaining popularity nowadays. It can transfer power in greater distance than IPT. In this section, a brief discussion of these methods has been presented.

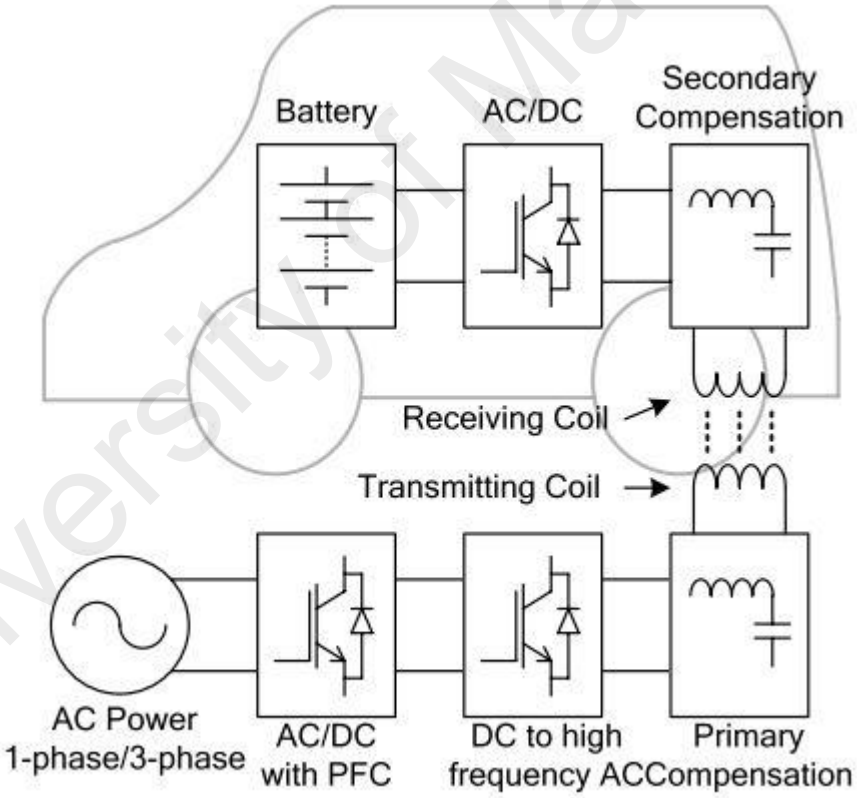

Figure 2.1: Wireless EV Charging System (schematic concept)

2.2.1 Inductive Power Transfer (IPT)

The conventional IPT system works on electromagnetic induction phenomena to transfer power through an air core transformer with closely spaced primary and secondary coils. This is much like electromagnetic induction used in the conventional iron-core

transformer. It offers very low efficiency when the gap between primary and secondary coil increases. Resonance techniques have been adopted on both side of the air-core transformer to alleviate this problem and the modified system is called resonance inductive power transfer (RIPT) or inductively coupled power transfer (ICPT) method. However, here, it will be referred as IPT to avoid confusion. IPT system can be used for small air-gap low power applications (1W to < 1 kW) as well as large air-gap (>10 cm) high power applications (> 1 kW) (Jiejian & Ludois, 2015). In most recent years, high power IPT has emerged as a means for EV charging application. A typical IPT system schematic for EV charging application is shown in figure 2.2.

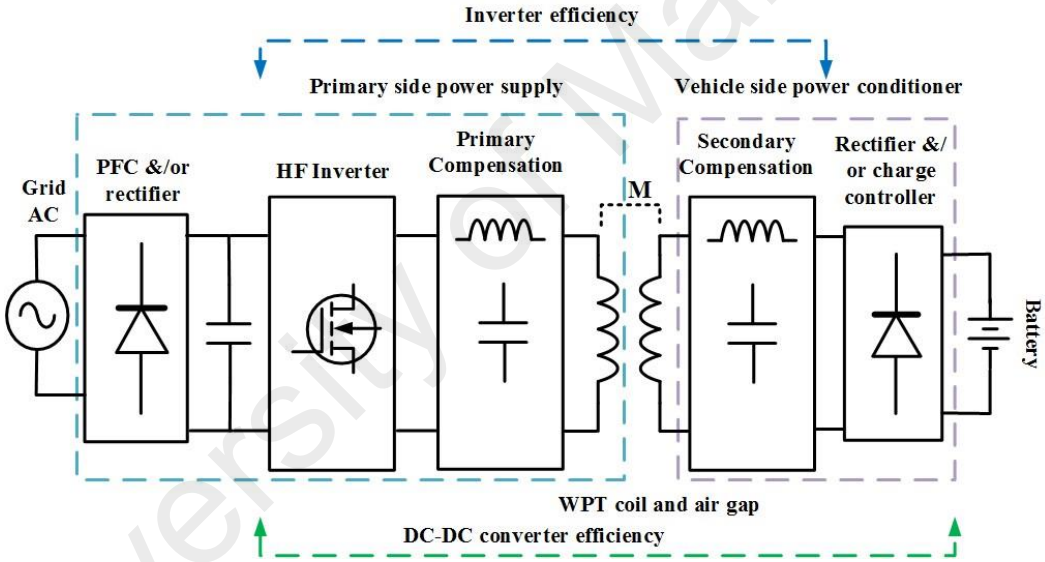

Figure 2.2: Electrical schematic of IPT system for EV charging

2.2.2 Capacitive Power Transfer (CPT)

The basic principle of CPT method is to utilize electric fields to transfer power, instead of magnetic fields within 100's kHz to 10's MHz frequency range. The electric fields can pass through metal barriers without generating significant power losses. The CPT method has shown promises in small air-gap and low power level applications (Jiejian & Ludois, 2015). However, this technology was overlooked over the last decades but in recent years, it has experienced rapid development. The power level and air gap of wireless CPT

system have been increased. Recent literature showed kW level power transfer with a large air gap (greater than 150 mm). Thus, wireless CPT method is now being considered as an alternative solution of IPT system for EV charging. Figure 2.3 shows the electrical equivalent schematics of CPT system.

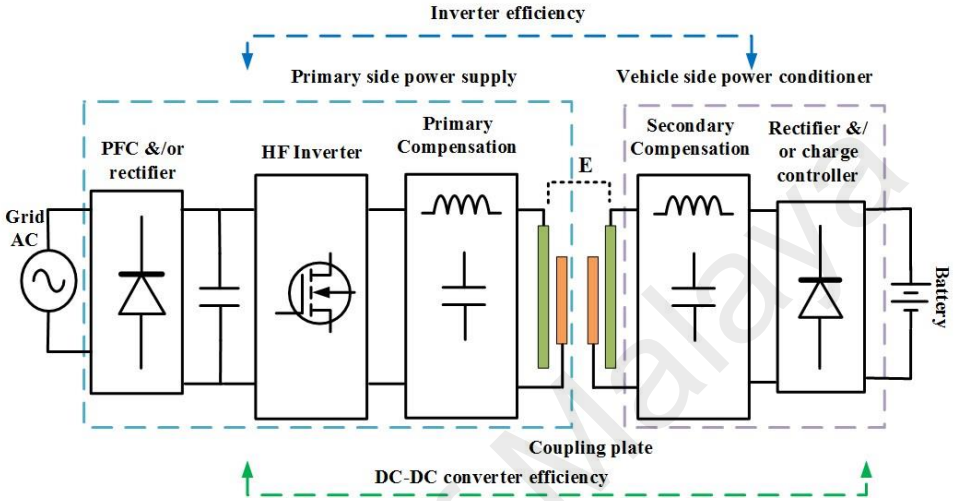

Figure 2.3: Electrical schematic of CPT system for EV charging (H. Zhang, Lu, Hofmann, Liu, & Mi, 2016)

2.2.3 Magnetic Resonance Coupling (MRC)

In MRC method, a strongly coupled magnetic regime is generated between primary and secondary coil. Power can be transferred effectively by tuning the coils to resonate at the same frequency. This method has gained research attention for WPT application since it has been introduced in 2007. A system was developed by MIT research group using MRC concept and it was capable of delivering power across 2m (meter) air gap (Kurs et al., 2007). The basic difference between the IPT and MRC methods is that the former uses a frequency range of up to 200 kHz and later uses MHz range frequency. Also, the IPT system has a coupling factor above 0.1 whereas in MRC method coupling factor is less than 0.1. Furthermore, ferrite core has been used for both the transmitting and receiving coils (to increase the magnetic coupling between the coils as the frequency is low) in the IPT system but the MRC system does not use ferrite core (Takanashi, Sato, Kaneko, Abe, & Yasuda, 2012). A schematic diagram of MRC system is shown in Figure

2.4. In the MRC system, source and load coil (A & B in figure 2.4) do not contribute to power transfer. So, by neglecting their effects MRC can be shown as a special form of conventional IPT system (Jin Huh, 2013). Despite potentiality, the MRC technology has not yet been actively put into the commercial purposes. The only available commercial product of this technology is WiT-3300 development kit released by WiTricity Corporation. It can deliver about 3.3 kW power at 180 mm with 90% efficiency.

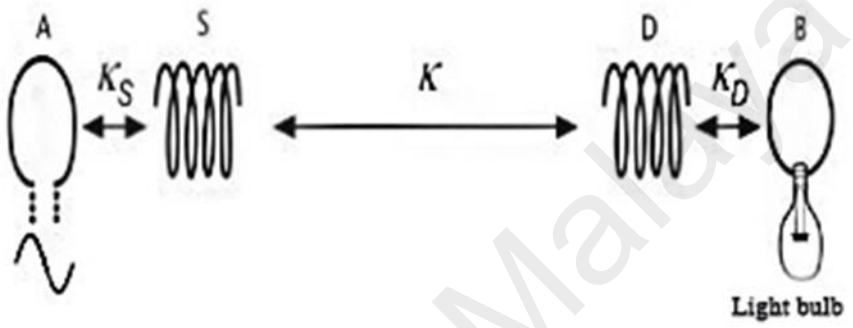

Figure 2.4: Schematic of four coil based MRC system (Kurs et al., 2007)

2.3 IPT for Contactless EV Charging System

It is predicted that future transportation systems will be dominated by electric vehicles (EVs) and plug-in hybrid electric vehicles (PHEVs). The decrease of fossil fuel reserves in various parts of the world as well as the adverse environmental effects of using fossil fuels are two main factors contributing to this prediction. Transportation causes the consumption of 27% world petroleum energy and 33.7% of greenhouse gas emissions in 2012 (Atabani, Badruddin, Mekhilef, & Silitonga, 2011; Tie & Tan, 2013). The EVs are solely operated by electric power and generates zero emissions of greenhouse gases. This helps to create a cleaner environment for all living around. EVs can be used in smart grid and smart house as bidirectional energy transfer system (Fukuoka et al., 2014). To make the EVs more attractive the charging system is a vital part.

A typical conductive charging scheme connects the vehicle-side (onboard) DC-DC converter input directly to a offboard DC-DC converter stage. This type of charging

system has some limitations such as hazardous accidental tendencies in rainy and snowy condition, bulk, lack of dynamic operation (charging while driving) etc. IPT based wireless charging can eliminate these limitations and at the same time provide high efficiency charging operations (both dynamic and stationary). As depicted in Figure 2.2, a typical IPT system is generally divided into two main sections: primary side or sending side and secondary side or receiving side. These two sections may include one or more power conversion stages based on practical implementation considerations. The IPT coils (sending and receiving) form/represents a transformer with a large air gap. Because of this air gap high leakage inductance is a common phenomenon of the IPT system. The high leakage inductance can be compensated using a resonant capacitor (Bosshard, 2015). Because of using compensation, a high efficiency is achieved even for a larger transmission distance. Therefore, by using IPT technique a contactless (wireless) charger can be designed which is capable to transfer high output power across the air gap that is standard for vehicle ground clearance (Bosshard, 2015; Bosshard & Kolar, 2016).

In summary, a wireless IPT vehicle charging system consists of an AC/DC converter at the primary side which converts utility alternating current (AC) power to a direct current (DC) power source, a high frequency inverter which converts the input DC power to high frequency AC, a compensation circuit and a transmitting coil. The secondary side an AC voltage is induced in the receiving coil by the high frequency alternating magnetic field due to the high-frequency current in the transmitting coil (both coils are tuned to the same operating frequency). This high-frequency AC power is then converted to DC via an AC/DC converter. The output of this AC/DC converter is then fed to a DC/DC converter which controls the charge to the battery and regulate the output voltage.

2.4 High Frequency (HF) Inverter for IPT EV Charging system

The primary side of Figure 2.2 can be further divided into following subsystems:

a) Grid input: 50/60 Hz AC power from grid which can be a single phase or three phases.
b) AC/DC rectifier: Converts utility input to a regulated DC voltage. In addition, it provides power factor correction and may work as a control mechanism for regulating power flow through the entire system (Esteban et al., 2015).
c) HF DC/AC inverter: A switching network which efficiently converts the incoming DC energy to high frequency alternating energy. It may be a full bridge, half-bridge, multilevel or single-switch type. The ON-OFF condition of the switches in the network is controlled by phase-shift scheme, frequency control scheme or both (Esteban et al., 2015). Usually, MOSFET is used as a switch because of their good high frequency characteristics. The switching network and compensation can be termed as resonant inverter.
d) Compensation network: A combination of low-loss (high Q) inductor-capacitor (LC) used after the switching network called compensation circuit. Commonly used compensation topologies are series (S), parallel (P), series-parallel(SP) and series-parallel-series (LCL/CLL). Compensation network helps to efficiently transfer power across the air-gap, reduce the VA rating of high frequency inverter and provides soft-switching of power semiconductor switch (Qu et al., 2017; W. Zhang & Mi, 2015).

These four blocks are commonly referred as a primary power supply in the literature (Bosshard & Kolar, 2016; Esteban et al., 2015). In this work, (c) and (d) are incorporated to define inverter topology for IPT EV charging. Other important issues of designing inverter for IPT EV charging system are frequency range and power level. According to the SAE J1772 standard, charging power level over 1 kW is termed as Level I and power level up to 19 kW is termed as Level II charger. These ranges are well suited for EV like small golf cart to medium size family car. On the other hand, high speed train and buses

required power level more than 20 kW (Bosshard, 2015; Bosshard & Kolar, 2016). The specific transmission frequency range for IPT EV charging system has not been fixed yet. Society of Automotive Engineers (SAE) has announced to specify a frequency band around 85 kHz in an upcoming standard J2954 for simplifying interoperability(Bosshard, 2015). In case of vehicle charging, 85 kHz is considered as high frequency compared to utility grid frequency, 50/60 Hz. Displacement and gating loss of power semiconductor devices and parasitic of various circuit components play very active roles during high-frequency operation (Perreault et al., 2009). Switching losses, large *dv/dt* and *di/dt* during switching operation and hence excessive EMI are some of the major limitations for existing hard switched PWM converters (Ching & Chan, 2008). Thus, conventional hard-switched PWM topologies are not suitable to meet such requirements. Therefore, combining (c) and (d), some special type of inverter topology can be obtained which are called resonant inverters. Resonant inverters are well suited to overcome the above-mentioned limitations of conventional inverters.

The basic principle of resonant converter is to control the transitions of the switches to occur at zero voltage or zero current points – ZVS (Zero Voltage Switching) and ZCS (Zero Current Switching) respectively - so that the switching losses are essentially eliminated. In general, full or quasi-resonance soft switching of a power switch occurs at one or more of the following four conditions (Hu, 2001).

1) Switching on and off at zero voltage points of a parallel capacitor. As the capacitor voltage cannot change instantaneously, and the time for the switches to turn on and turn off is relatively short, ZVS can be approximately achieved.
2) For the similar reason, as 1), switching on and off can occur at zero current points of a series inductor due to the slow rate of change of current (di/dt) at that point. Consequently, approximate ZCS can be achieved.

3) Switching on and off at zero voltage when a parallel diode is conducting. The anti-parallel body diodes of many power switches, such as those of MOSFETs and IGBTs, are often used for this purpose.

4) Switching on and off at intervals of a discontinuous current mode. As the circuit is equivalent to an open circuit during a discontinuous current period, ZCS or ZVS may be achieved.

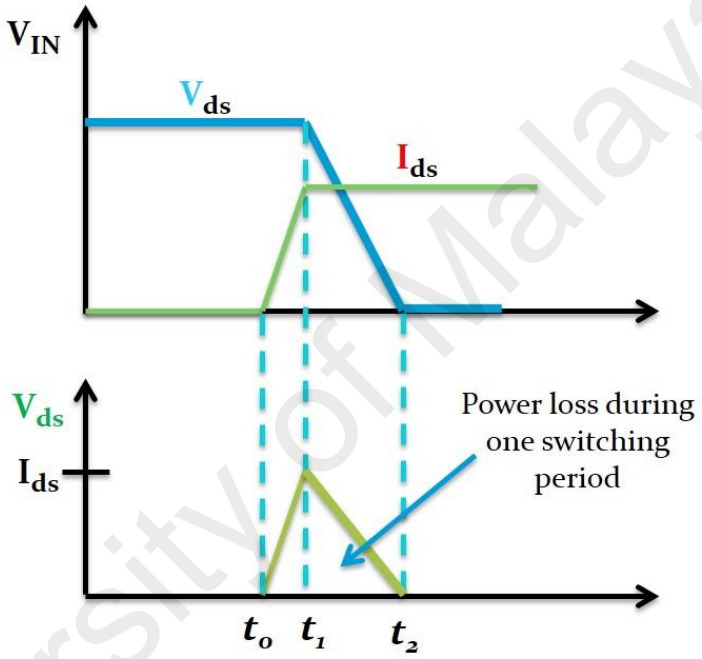

Figure 2.5: Drain-to-Source voltage and current waveform of a converter switch during the off-to-on transition while driving at hard switched method.

Designing of resonant inverters are challenging due to the complexity of the circuit. This is mostly because of introducing additional reactive components to achieve soft switching. However, these types of inverter topologies are becoming very popular in the IPT application because of their significant contribution to switching loss reduction, better waveform generation and especially compatibility with IPT system specification.

2.5 Compensation topologies for IPT System

Compensation plays an important role in IPT system and as an integral part of resonant inverters. It helps to increase overall system as well as inverter efficiency. It provides the reactive power required for the primary coil to generate an adequate magnetic field which in turns minimize the VA rating (Sallan, Villa, Llombart, & Sanz, 2009; W. Zhang & Mi, 2015; W. Zhang, Wong, Tse, & Chen, 2014) of the inverter hence overall power supply scheme. A well-designed compensation topology could provide constant voltage/current characteristics during a certain percentage of coil misalignments, coupling and load variation of an IPT system.

In an IPT system, two parameters: the coupling coefficient and the quality factors of the windings decide the maximum achievable system efficiency. An adequate compensation is necessary to achieve the maximum efficiency. Moreover, it also helps to achieve soft switching of the power semiconductor switches of the resonant inverter. In the case of MOSFET, zero voltage switching (ZVS) can be achieved by proper tuning of the inverter. Thus, switching losses are reduced during high-frequency operation. Finally, properly tuned compensation eliminates the bifurcation phenomenon of a WPT system. It is necessary to avoid bifurcation phenomenon in a WPT system to guarantee system stability. However, for evaluating compensation topology, with the aforementioned compensation purposes some special features like insensitivity to parameter change and suitability for bi-directional power flow should also be considered their applications and expected operations. Common compensation topologies implemented by the researcher so far have been described in the following section. Besides these, some new family of compensation topologies have been described in a current literature (Qu et al., 2017). However, further research and experiment are required to determine the feasibility and performance of those topology in IPT system

2.5.1 Common Compensation Topologies

Figure 2.6 shows four common compensation topologies for IPT system. They are SS, SP, PS and PP compensation. Here, the first term indicates the type of primary compensation capacitor connection and second term indicates the type of secondary compensation capacitor connection. Furthermore, 'S' is used here for 'series' and 'P' is used for denoting 'parallel'.

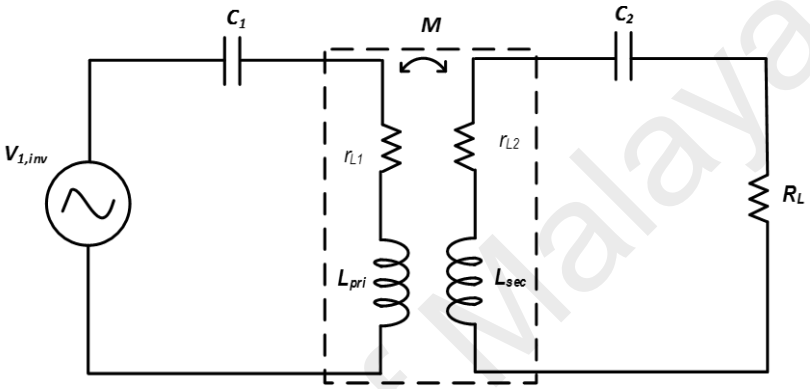

(a)

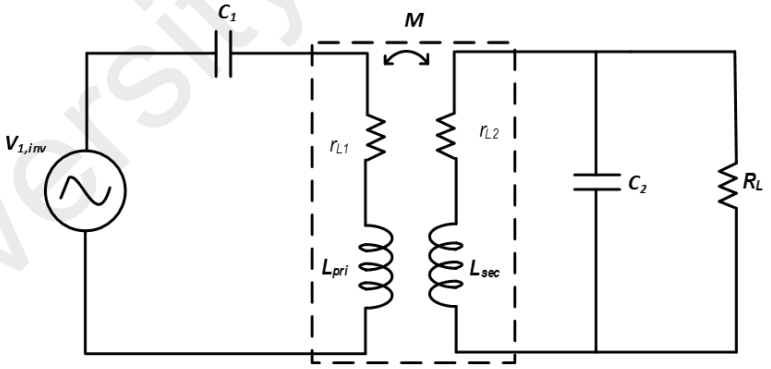

(b)

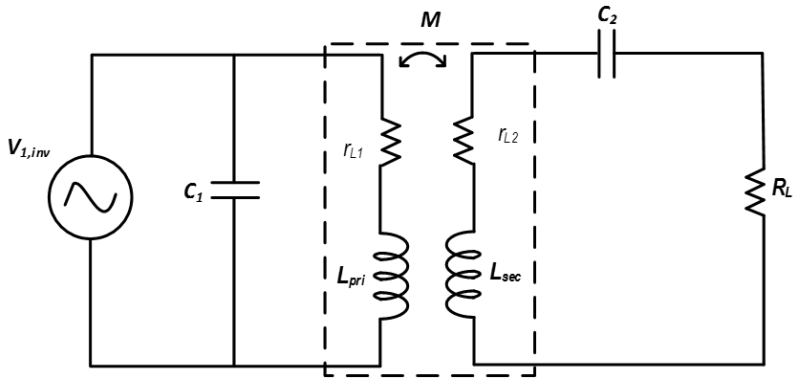

(c)

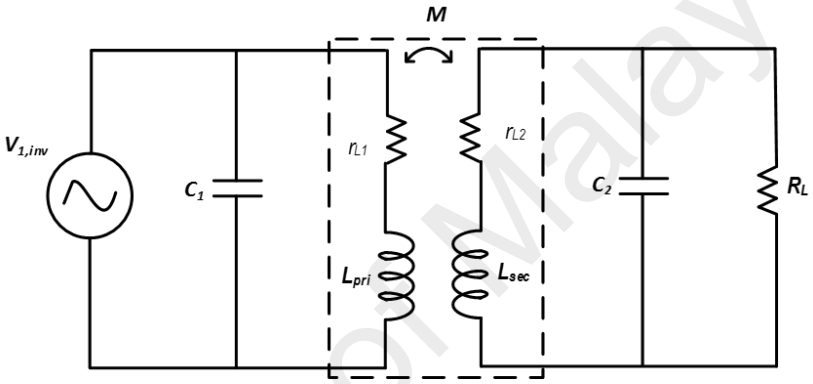

(d)

Figure 2.6: Commonly used compensation topologies (a) SS (b) SP (c) PS (d) PP

A simplified model of IPT EV charging system with HF inverter has been shown in figure 2.7. Fundamental frequency component has been assumed to construct this simplified model. Due to a high-quality factor of the IPT coils fundamental frequency component analysis can obtain straightforward and accurate analytical result. In this model, secondary impedances have been reflected to the primary for calculating overall VA rating and efficiency of the inverter.

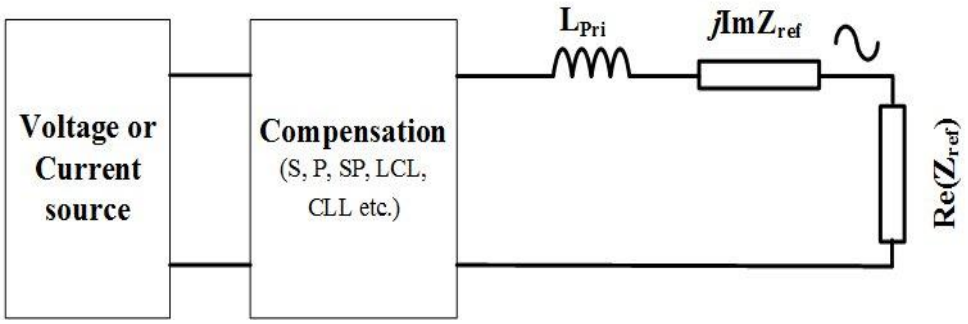

Figure 2.7: Simplified model to design HF resonant inverter for IPT EV charging

The total impedance seen by the inverter for above-mentioned compensation topologies can be expressed in the equations 2.1 – 2.4 (Pinuela, Yates, Lucyszyn, & Mitcheson, 2013; Sallan et al., 2009).

$$Z_{ss}(\omega t) = (r_{L1} + j(\omega L_{pri} - \frac{1}{\omega C_1})) + \frac{\omega^2 M^2}{(r_{L2}+R_L+j(\omega L_{sec}-\frac{1}{\omega C_2}))} \quad (2.1)$$

$$Z_{SP} = (r_{L1} + j(\omega L_{pri} - \frac{1}{\omega C_1})) + \frac{\omega^2 M^2}{(r_{L2}+j\omega L_{sec}+\frac{R_L}{1+ j\omega C_2 R_L})} \quad (2.2)$$

$$Z_{PS} = \frac{1}{(r_{L1}+j\omega L_{pri})+\frac{\omega^2 M^2}{(r_{L2}+ R_L+j(\omega L_{sec} - \frac{1}{\omega C_2}))}+j\omega C_1} \quad (2.3)$$

$$Z_{PP} = \frac{1}{\frac{1}{(r_{L1}+j\omega L_{pri})+\frac{\omega^2 M^2(1+j\omega C_2 R_L)}{(R_L+(r_{L2}+j\omega L_{sec})(1+j\omega C_2 R_L))}}+ j\omega C_1} \quad (2.4)$$

Here, L_{pri}, L_{sec}, r_{L1} and r_{L2} are primary and secondary coil main inductance and parasitic inductance respectively. C_1 and C_2 are primary and secondary compensation capacitor. R_L is AC equivalent load resistance.

To model the reflected equivalent secondary side impedance, the secondary compensation circuit must be determined. Usually, two types of compensation for the WPT secondary or pickup side have been discussed popularly in the literature: series compensation and parallel compensation. Secondary series compensation is achieved by

placing a capacitor in series with secondary leakage inductance and parallel compensation is obtained by placing the capacitor in parallel (Miller, Onar, & Chinthavali, 2015; Ning, Miller, Onar, & White, 2013; Onar et al., 2014; Sallán, Villa, Llombart, & Sanz, 2009). Uses of series and parallel compensation and their performance analysis for optimal efficiency, load independent voltage transfer ratio, the specification of application and coupling insensitivity have been investigated in various studies and references therein (W. Zhang et al., 2014).

2.6 Popular Resonant Inverter Topologies for IPT EV charging

IPT EV charging system requires power level 2 kW and higher. Thus, researchers dominantly used bridge configuration with series LC resonant (SLC) and series-parallel resonant (LCL/LCC) topologies. However, a single switch class E resonant inverter and its variant could also meet the requirements of the WPT system because of its ability to deliver medium power (1-3 kW) at higher switching frequencies (Aldhaher, 2014a; Aldhaher, Luk, et al., 2014b; Yusmarnita Yusop, 2016). In this section, a couple of popular inverter topologies will be discussed based on previous literatures. Single switch inverter will also be described to address the research goal of this work.

2.6.1 LCL/LCC Resonance Based Inverter for IPT System

Comprehensive work has been done for IPT system to use Inductor-Capacitor-Inductor (LCL) load resonant inverter (Hao, Covic, & Boys, 2014; Huang, James, & Covic, 2015; Kissin, Huang, Covic, & Boys, 2009) which uses four switch bridge topologies, the output of which is fed into an LCL resonant circuit. This LCL resonant circuit is formed by a series inductor primary, a parallel compensation capacitor, after the bridge network of power semiconductor switch and primary coil inductance. It can also be called an LCLC configuration. In figure 2.8, an LCL primary based IPT system has been depicted.

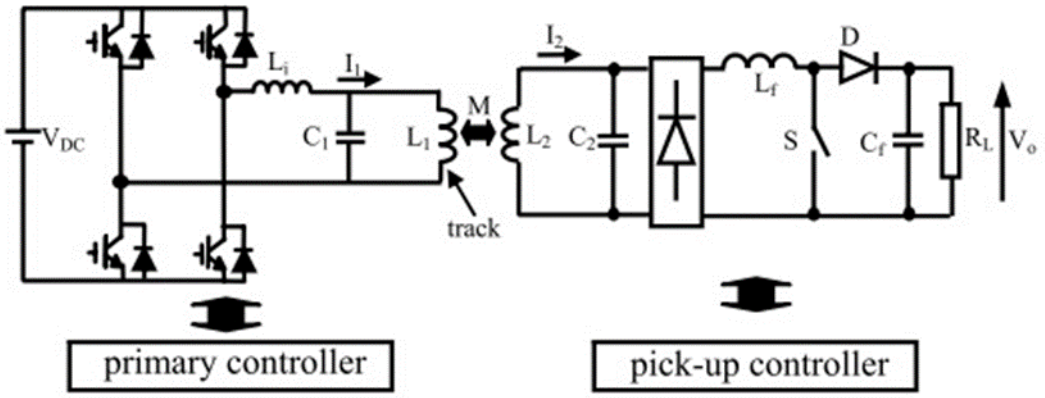

Figure 2.8: Bridge configuration & LCL primary compensation based IPT system

A 5 kW inductive charger is also reported in (Wu, Gilchrist, Sealy, & Bronson, 2012) using the same type of resonant inverter. The output frequency of this inverter was 20-30 kHz. In primary inverter phase shift control was implemented to control the track current. It presented dual control method for optimizing system efficiency. In (Huang et al., 2015) primary side bridge configuration with LCL compensation was proposed for multiple secondary pickup WPT systems. This system can work well in a variable coupling condition.

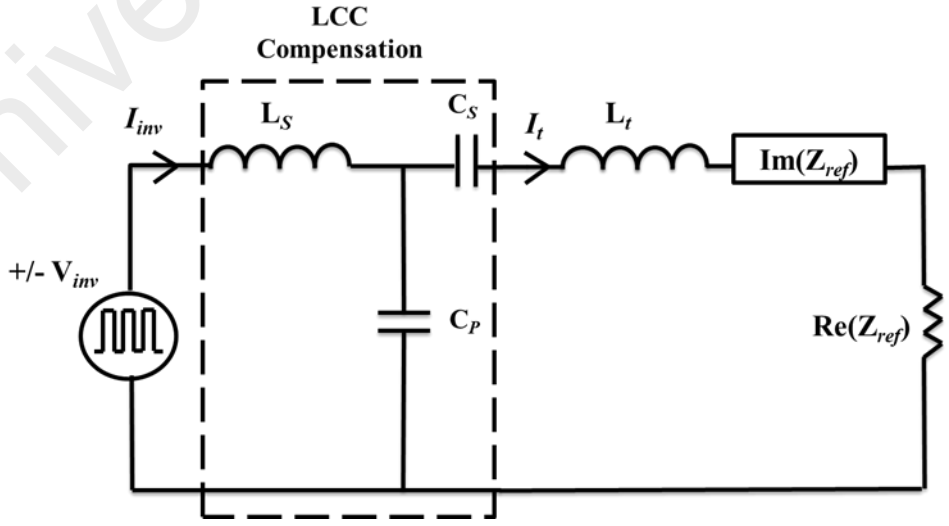

Figure 2.9: Simplified FHA based IPT system model using LCL/LCC compensation

A simplified analytical load modelling for LCL compensated primary has been proposed in this work. Figure 2.9 shows the overall system modelling based on this method. Madawala and Thrimawithana (2012) proposed a promising LCL based primary side bridge inverter for IPT system by using the same topology.

2.6.2 Series Resonance (LC or SLC) Based Inverter for IPT System

Another widely used power supply (or inverter) topology for IPT system is series resonance based soft switching inverter. In this topology (figure 2.10), a series capacitor is used with bridge configuration which acts as primary compensation and provides soft-switching assistance for inverter power semiconductor switch. A series compensated high-performance SiC MOSFET based bridge inverter has been developed by Oak Ridge National Laboratory (ORNL). This inverter has been tested for frequency up to 142 kHz. In a recent publication (Miller et al., 2015) ORNL also presented a primary side power flow control method by varying frequency and duty cycle of the primary side inverter with an efficiency more than 85%.

Moreover, a 3 kW primary series compensated inverter is designed (Diekhans & De Doncker, 2015) and tested with more than 92.1% efficiency. An effective dual side control method has been implemented on this system. Some recent literature (Bosshard, Badstubner, Kolar, & Stevanovic, 2012; Bosshard et al., 2015; Bosshard, Kolar, & Wunsch, 2014) also presented this topology with higher efficiency during misalignment and variable loading condition. Both topologies have its own advantages during misalignment, partial loading and coupling variation. LCL based fixed frequency control has small dc bus capacitor, which offers good input power factor (Hao et al., 2014). Its constant operating frequency eliminates bifurcation (Huang et al., 2015) and simplifies tuning of secondary pickups. Also, its steady-state track current is load independent. This greatly simplifies the control and regulation of power for an IPT system.

Soft switching of the semiconductor switch can be achieved. Thus, reduced switching loss is obtained during high-frequency operation. In the case of series compensation (figure 2.6a), the compensation capacitor is independent of magnetic coupling or the load. It can be shown in equation (2.5) (Bosshard et al., 2012). The system exhibits a low sensitivity to coil misalignment, and the resonant frequency of the resonant circuit is constant, provided that there is a small component tolerance in the system. Zero current switching (ZCS) for the rectifier diodes on the receiver side is achieved using this compensation topology.

$$C_1 = \frac{1}{\omega_0^2 L_1} \quad \text{and } C_2 = \frac{1}{\omega_0^2 L_2} \tag{2.5}$$

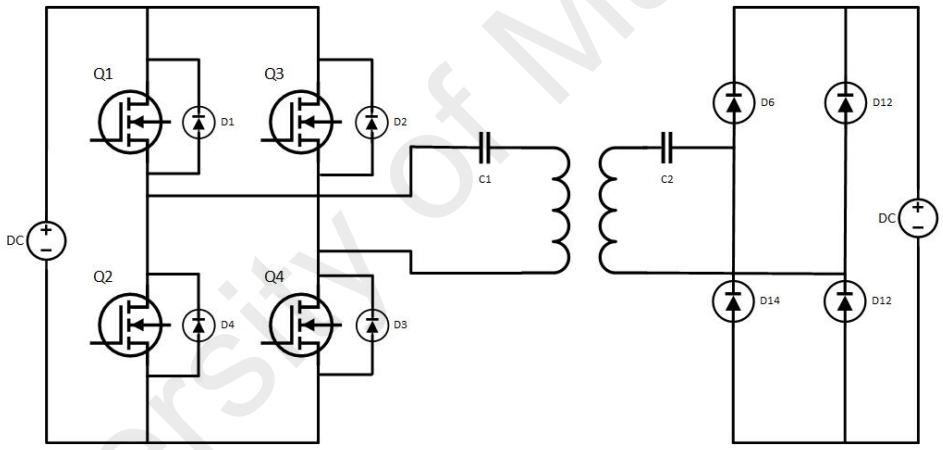

Figure 2.10: Series compensation based IPT system

2.7 Single Switch Resonant Inverter for IPT System

A single switch class E resonant inverter can also meet the requirements of the WPT system because of its ability to deliver medium power (1-3 kW) at higher switching frequencies (Aldhaher, 2014a; Aldhaher, Luk, et al., 2014b; Yusmarnita Yusop, 2016). Class E resonant inverter is capable of high-frequency operation (hundreds of kHz to several MHz) with high efficiency by maintaining zero voltage switching (ZVS) and zero slopes switching (ZdVS). This inverter also has a simple topology with lower component

count and timing control, and require a relatively simple gated drive because of the absence of high and low side complimentary switches.

2.7.1 Current-Fed Class E Resonant Inverter

Figure 2.11 and 2.12 show the current-fed class E resonant inverter topology and operating waveform during nominal condition. This inverter was first introduced by Sokal (Sokal & Sokal, 1975). A conventional current-fed class E inverter usually consists of dc-supply $V_{IN(DC)}$, input choke (dc-feed) inductance, L_{choke}, power MOSFET as switching device, a shunt capacitor, C_P, and a load circuit (combination of series resonant circuit L_S-C_S and ac load resistance, R_L).

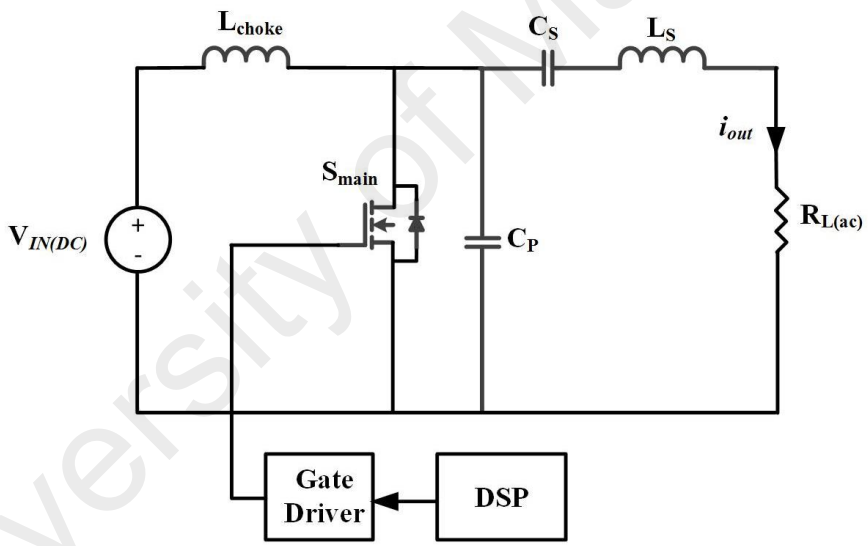

Figure 2.11: Current-fed class E inverter.

During nominal operation, class E inverter maintains zero-voltage switching (ZVS) and zero derivative switching (ZDS) simultaneously. Thus, it achieves high power-conversion at higher frequencies. Switching loss also reduce significantly because of zero-voltage and low transient overcurrent at turn-on instance. The ZVS/ZDS condition is expressed in equation (2.6).

$$v_{DS(2\pi D)} = 0 \text{ and } \frac{dv_S}{d(\omega t)}(\omega t) = 0 \tag{2.6}$$

Where, $\omega t = 2\pi D$. These conditions are referred as "nominal condition" for class E inverter operation. In case of maximum power conversion efficiency, conduction losses for components ESR and switch-on/off time resistance must be considered. This operating condition including ESR is referred as "optimal condition". The nominal operating waveforms of class E inverter at D = 0.5 (duty cycle) have been depicted in figure 2. The difference of currents through the dc-feed inductance (or choke inductance), L_{choke}, and resonant network (L_S-C_S) flows through the capacitor C_P during switch turn-off interval. Operating frequency is selected to be greater than the resonant frequency of L_S-C_S but less than the resonant frequency of L_S-C_S-C_P. Furthermore, output resonant circuit of class E inverter usually has a high-quality factor, Q. Thus, load current, i_{out}, is regarded as a sinusoid.

Major advantages of class E inverter are less component count, simple gate drive configuration, inherent sine-wave voltage/current output and efficient high frequency operation due to ZVS/ZDS. ZDS operation reduces Miller effects. Class E inverter topology has been discussed for planar WPT (Aldhaher, 2014a; Pinuela et al., 2013), wireless powering for biomedical devices and vehicle charging applications (Aldhaher, 2014a; Aldhaher, Luk, et al., 2014b; Fukuoka et al., 2014). Despite these significant advantages, it also porn to few severe cons. Foremost is the peak switch voltage stress across semiconductor switch. It is shown in Figure 2.12 that drain-to-source voltage, V_{DS}, is 3-3.5 times the input DC voltage. In high-power and high-frequency condition this phenomenon is not desired. Another major disadvantage of class E inverter is that input dc-feed inductor loss is high because it's size is bulky. Thus, core loss and ESR loss is high. In case of usability with IPT system, Class E inverters are sensitive to load variations because to achieve ZVS and ZdVS conditions component values are chosen uniquely. Any change in the load impedance would cause the inverters to deviate from its optimal operation hence ZVS and ZdVS switching conditions cannot be maintained. This will

cause high switching losses and stress to the power MOSFET which leads to device failure.

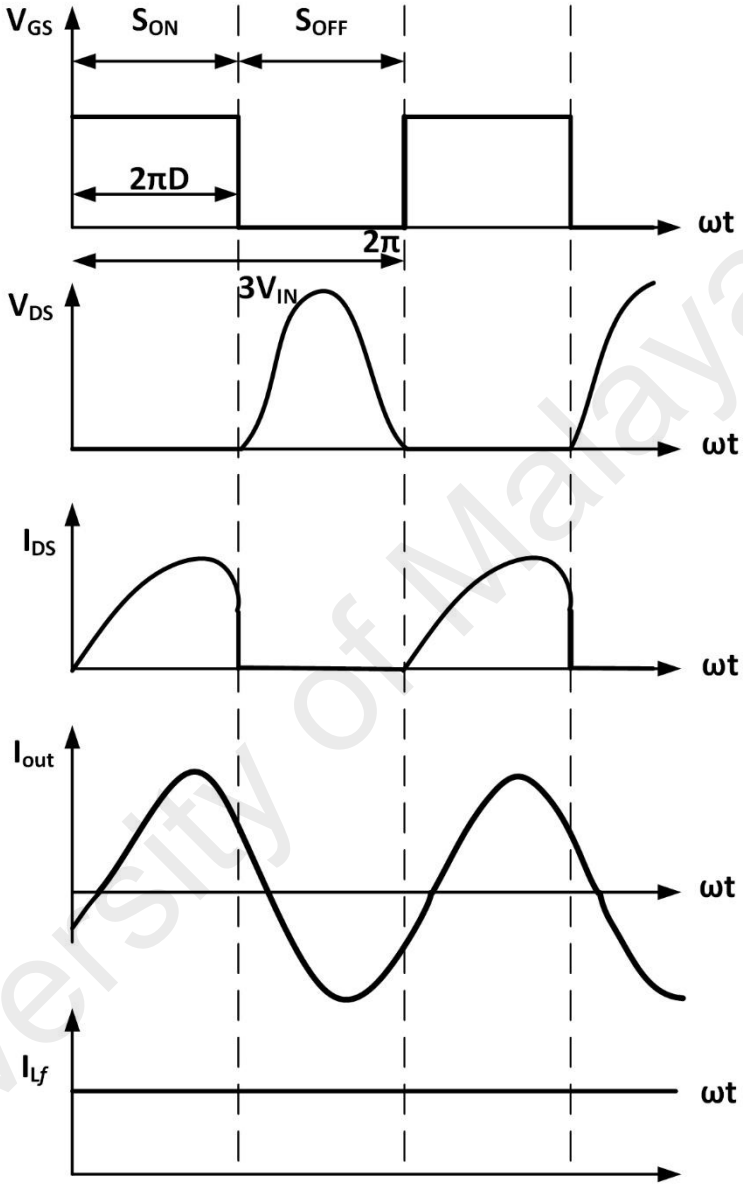

Figure 2.12: Nominal operating waveforms of current-fed class E inverter (D = 0.5).

To overcome this problem an electronic tuning method using saturable reactors is presented in (Aldhaher, Luk, et al., 2014b) to deal with impedance variation caused by WPT coil misalignment and relative distance and is suggested for IPT vehicle charging

applications. A numerical design method by using implicit circuit equation has been presented in (Nagashima, Xiuqin, Suetsugu, Kazimierczuk, & Sekiya, 2014) which allows the overall WPT system design using Class E inverters without considering impedance matching and a parameter of the system. A 7^{th} order piecewise linear state-space modelling of Class E inverter and rectifier was also presented in (Luk, Aldhaher, Fei, & Whidborne, 2015) recently for WPT application. This model can also obtain several WPT parameters and values to ensure optimum switching operation of Class E inverters. Although these solutions eliminate some of the cons of class E inverter, they also introduce complexity and extra component count which may not be suitable for commercial implementation.

2.7.2 Variant of Class E inverter

To overcome the limitations of class E inverter some new topologies have been proposed over the last few years. It has been reported in (S. Aldhaher et al., 2015; Kaczmarczyk, 2006; Kee et al., 2003; Mediano & Sokal, 2013) that the efficiency of the Class E inverter can be improved and its voltage or current stresses can be reduced by adding a resonant network either in parallel or series to its load network. The added resonant network or networks could be in the form of a series LC lumped network that is connected in parallel with the load network as shown in a parallel LC lumped network that is connected in series with the load network as shown in or a combination of both series and parallel LC lumped networks that are connected in series and in parallel with the load network as shown in (S. Aldhaher et al., 2015). A $\lambda/4$ transmission line that is inserted between the supply source and the inverter can be also be used as shown in (Rivas et al., 2008).

The method of adding resonant networks to the load network is used in Class F and Class F-1 inverters, and by applying it to the Class E inverter results in a hybrid inverter

which has been referred to as the Class EF_n or Class E/F_n inverter. The subscript n refers to the ratio of the resonant frequency of the added resonant network to the switching frequency of the inverter and is an integer number greater or equal than 2. The 'EF_n' term is used if n is an even integer and the 'E/F_n' term is used if n is an odd integer. These types of inverters can reduce the power semiconductor switch stress significantly.

It is seen that switch stress of these inverters are 40-45% less from typical class E inverter. Thus, power handling capability is also improved. Figure 2.8 depict a class EF_n topology. It is also noted that class EF_n also termed as class Φ_2 in (Rivas et al., 2008). The difference lies in the fact that the Class φ2 inverter uses a finite input choke (L_F in figure 2.12) as opposed to an infinite inductance input choke in the Class EF inverter. Using a finite inductance input choke makes the choke a part of the load network and has the effect of increasing the maximum switching frequency of the inverter. This is the case of the 'Class E inverter with finite DC-feed inductance' where the maximum switching frequency of a Class E inverter is increased by a factor of approximately four by using a finite inductance input choke (S. Aldhaher et al., 2015).

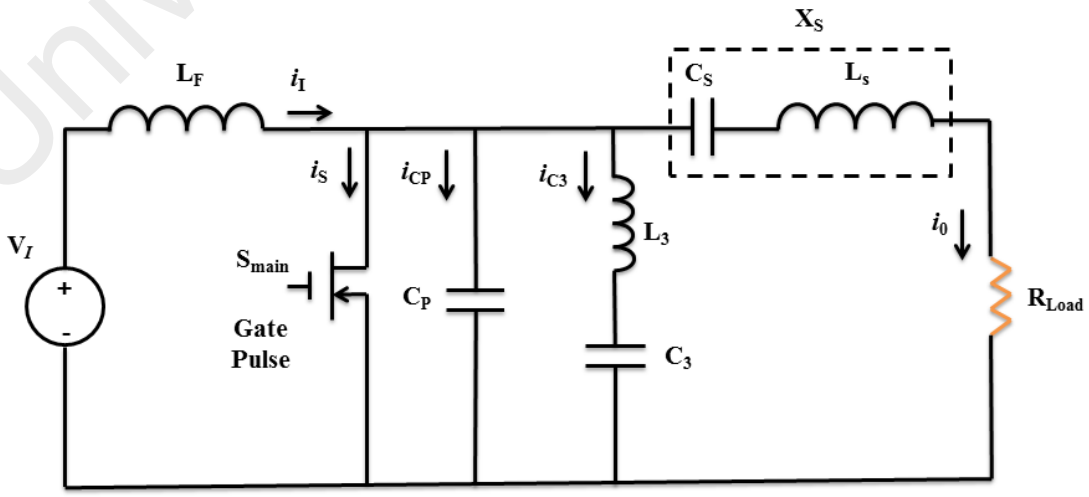

Figure 2.13: Circuit diagram of Class EF_2 or class Φ_2 inverter

Different numerical methods have been presented to analyze these inverters operation. However, implementing as IPT primary side inverter requires different tuning procedure. Some design procedures have been discussed in recent literature in the quest of implementing these inverters to IPT system. However, different types of tuning procedures can be explored to incorporate them in IPT system.

2.8 Control of Primary Side Inverter

Controlling of primary side inverter for the IPT EV charging system is challenging. Variation of magnetic coupling, misalignment, output power and output voltage regulation are the main factors for EV charging control design. Possible control methods include a variation of either the phase shift between the two converter bridge legs, the switching frequency or the dc-link voltage. An additional buck stage is required for controlling the dc link voltage. Common control methods discussed in the literature so far are phase shift control, frequency control, and dual side control. Bosshard et al. (2012) showed different control method for a series-parallel compensated IPT system. A comparative evaluation of current and voltage stress in the transmission coils, the resonant capacitors and the power semiconductor switches in the primary-side inverter is presented. Finally, a dual control method was proposed. Three possible control methods, a) phase shift control at a fixed switching frequency, b) frequency control, and c) dual control, are discussed and evaluated. Main criteria for the evaluation of these control technique was: efficiency, component stress and controllability of the power electronic system.

A possible control scheme for a full-bridge inverter is the operation at a constant switching frequency "f_s" with a variable phase shift of the two bridge legs. This allows producing an inverter output voltage with a variable pulse width and, thus, a variable amplitude of the fundamental. Theoretically, this would offer the possibility to control

the output power of the resonant converter. However, applying this control method aggravates ensuring soft-switching of the semiconductor devices, because the inductive operation is not guaranteed near the resonant frequency if a pole-splitting occurs. Therefore, high switching losses resulting from reverse recovery of the anti-parallel diodes occur. Additionally, the reduction of the voltage amplitude requires a higher primary current to deliver the same amount of power to the load. This results in an increase of the conduction losses in the switches and the resonant circuit and the system efficiency would be reduced.

In dual control scheme, phase shift and frequency control are combined. The zero crossings of the primary current are detected and used to trigger the gate signals for the switches of the leading bridge leg. After the active interval determined by the duty cycle D, the switch of the lagging bridge leg is turned off and the current is commutated to the anti-parallel diode of the opposite switch, which can, therefore, be turned on while the diode is conducting. As a result, the leading bridge leg is operated with Zero Current Switching (ZCS) and Zero Voltage Switching (ZVS) at turn-on and turn-off. The lagging bridge leg is operated with ZVS at all switching instants.

A controlled rectifier can be used in the input stage of single switch modified class E inverter. It not only results in a regulated voltage supply but also allows it to be controlled and varied according to the operating conditions of the IPT system. Since variations in the distance between the coils of the inductive link are likely to occur, the input voltage to the Class E inverter may have to be adjusted to transfer a specific amount of power to the rectifier and the load.

One comparator based control scheme has been presented for class E inverter (Aldhaher, 2014b). The comparator will provide a positive output if the output voltage of the converter is below the reference voltage and a negative output if the output voltage is

above the reference voltage. Depending on the output of the comparator, the counter will count when the output of the comparator is positive, which will cause the duty cycle to increase leading the output voltage to rise towards the reference voltage. The counter will count down when the output of the comparator is negative causing the duty cycle to decrease, which leads the output voltage to decline to the reference voltage. For each count, the counter either increments or decrements the duty cycle by a minimum step and the clock of the counter set the time interval between the counts.

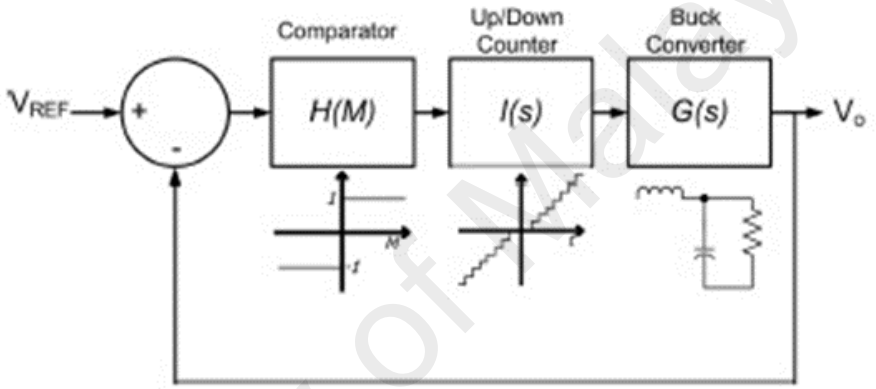

Figure 2.14: One comparator based control scheme (Aldhaher, 2014b)

2.9 Summary

The variants of class E inverter has good potentiality in IPT system. In contemporary literature, to the best of author's knowledge, detailed designs of these types of inverters are confined to the frequency range between 800 kHz to 13.6 MHz, even though some WPT applications operate on a 20 kHz–100 kHz frequency range (Aldhaher, Yates, & Mitcheson, 2016; Sokal & Sokal, 1975). Therefore, a clear scope for evaluating the performances of these types of inverters under above frequency constraint exists. In this work, a modified class EF_2 voltage-fed multi-resonant single switch inverter topology has been proposed for IPT applications. A medium frequency (85-100 kHz) region with practical IPT coil parameters is used to evaluate the performance and effectiveness of the inverter. The proposed inverter has all the advantages of class E inverter. The following

chapters will describe the design of proposed inverter, simulation, prototype, experimental result, and discussions.

CHAPTER 3: VOLTAGE-FED MODIFIED CLASS EF_2 INVERTER

3.1 Introduction

The main objective of this research is to design and investigate the performance of a modified class EF_2 inverter. A complete mathematical modelling and calculation of inverter component values will be the focus of this chapter.

3.2 Series Compensated Reflected Impedance

Series compensated secondary has constant voltage source characteristics (Diekhans & De Doncker, 2015; Jia, Qianhong, Siu-Chung, Tse, & Xinbo, 2015; W. Zhang, Wong, Tse, & Chen, 2013) and has been considered here for stationary vehicle charging (SVC) applications. Although it imposes a difficulty of matching induced secondary coil voltage (pick up voltage) to desired output voltage this could be eliminated with a proper secondary voltage control circuit. In the case of stationary vehicle charging, primary and secondary coil misalignment can be assumed negligible hence the detuning effect of the secondary compensation circuit will be negligible. A series compensated secondary with primary side current control could be employed for the battery electric vehicle (BEV) wireless charging (a stationary vehicle charging is also called BEV (Kalwar, Aamir, & Mekhilef, 2015)). For a primary current control system, a simple series compensated secondary can be designed as shown in figure 3.1(a) which consists of a pickup coil, a series capacitor, a bridge rectifier with dc filter and battery or load. The simplified LCR model of this pickup circuit is shown in figure 3.1(b) in which R_L is an equivalent ac resistive load to represent the dc battery of EV, rectifier and filter capacitor and $V_{S\text{-}OC}$ is the secondary open circuit voltage (Huang, Boys, & Covic, 2012; Huang et al., 2015). From figure 3.1(b) the impedance seen by the secondary open circuit voltage $V_{S\text{-}OC}$ is $Z_{S\text{-}S}$ and it can be calculated as follows:

$$Z_{(ss)} = R_L + j\omega L_{sec} + \frac{1}{j\omega C_2} \tag{3.1}$$

In a practical implementation, the secondary circuit is usually kept in resonance. Hence using equation (3.1) and the theory of magnetically coupled circuit, the reflected impedance of series-compensated secondary is given by:

$$Z_{r(ss)} = \frac{\omega^2 K^2 L_{pri} L_{sec}}{R_L} \tag{3.2}$$

Here, "*K*" is the coupling coefficient, L_{pri} and L_{sec} are sending and receiving coil inductances.

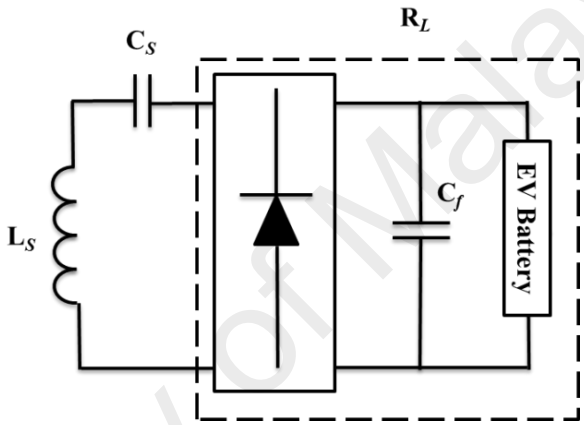

(a)

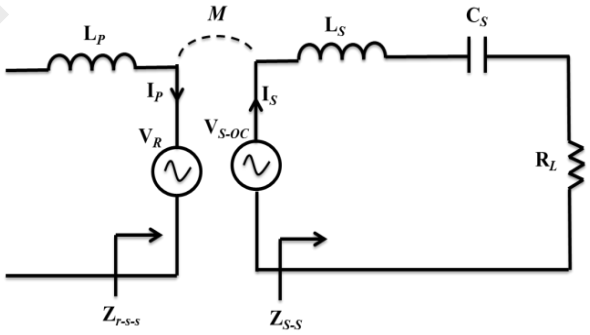

(b)

Figure 3.1: (a) Series-compensated secondary or pickup model (b) Simplified series-LC secondary for calculating secondary reflected impedance to the primary side

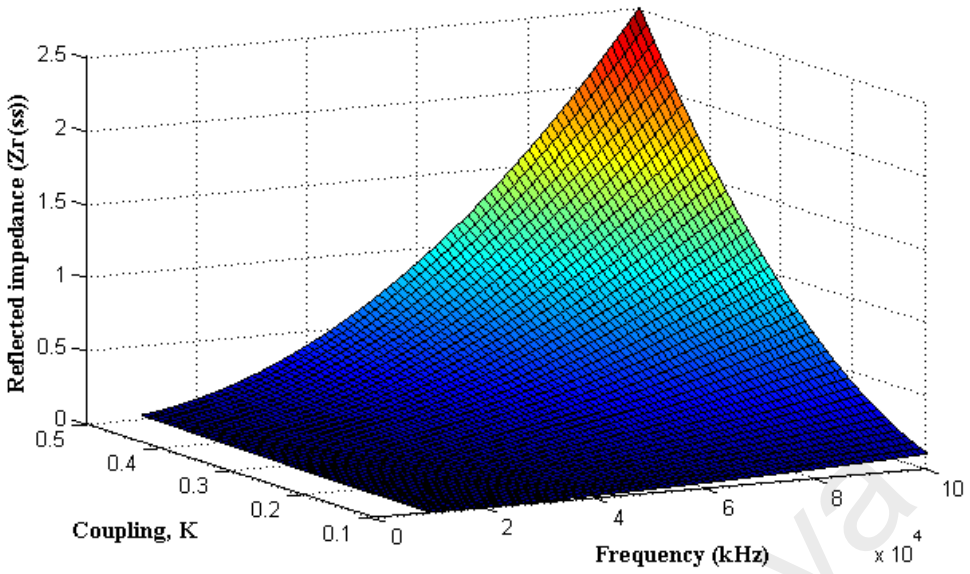

Figure 3.2: Secondary series reflected impedance variation depending on K and frequency

3.3 Voltage-Fed Modified Class EF_2 Resonant Inverter

The proposed inverter topology has been depicted in figure 3.3. Here, input dc-feed inductance is replaced with a resonant inductance L_R. In class E inverter, the input dc-feed choke inductance is bulky and produce high losses while operating in a frequency region of 30 – 100 kHz. This loss has been substantially reduced for using a resonant inductor. As this inductor now resonates with a higher frequency than switching frequency so volume and value of the inductor have been reduced. Thus, small core area is required to construct it with less turn. This will lead to a small magnetic and ESR loss.

Furthermore, to reduce the peak voltage stress across the switching device a series resonant circuit (L_{SR} - C_{SR}) has been inserted between input resonance inductor and switch. This series resonant circuit is tuned to resonate with the second harmonic of the switching frequency. The idea of using the extra resonant circuit with selected harmonic elimination for reducing switching stress has been discussed comprehensively in (S. Aldhaher et al., 2015; Kaczmarczyk, 2006; Phinney et al., 2007; Rivas et al., 2008). The second harmonic elimination contributes to reducing peak switch voltage stress. For a

class E current source inverter, the maximum peak voltage across the switch can reach up to 3.5 times to the input DC voltage. Whether, in the proposed multi-resonant inverter, the voltage peak is limited to only 2 times of input DC which is shown in following sections. This peak switch stress reduction is necessary for using the high input DC (rectified from utility). In case of conventional class E, if a rectified voltage of 300 V is applied the peak switch-stress will go up to 1kV which is not desirable. On the other hand, in case of the proposed inverter it will reach up to 600V. This is well in the range of safe operating area (SOA) of the switch. Furthermore, there are lots of commercial semiconductor switch available for practical implementation of the inverter.

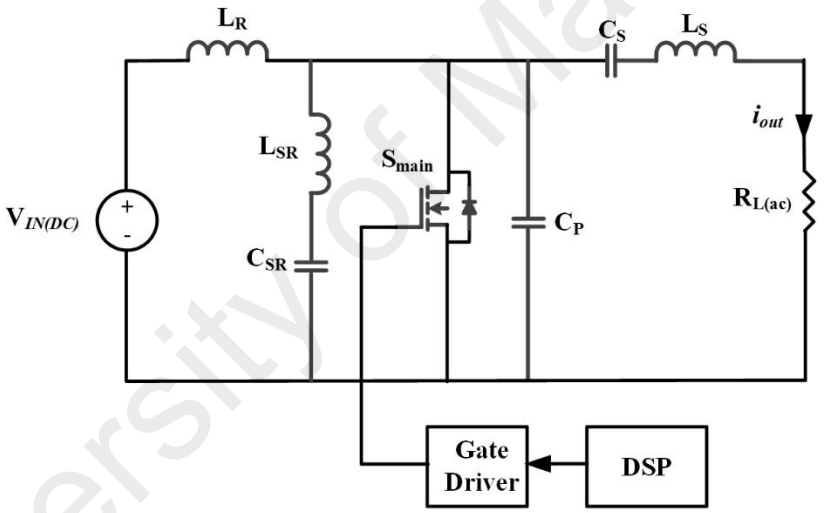

Figure 3.3: Proposed voltage-fed multi-resonant class EF_2 inverter.

The components of the inverter are calculated such that the peak voltage amplitude across the switch becomes low and maintains switch-mode operation through near zero-voltage at turn-on and turn-off at a given frequency and duty ratio. Figure 3.4 shows a simplified circuit diagram of the proposed inverter.

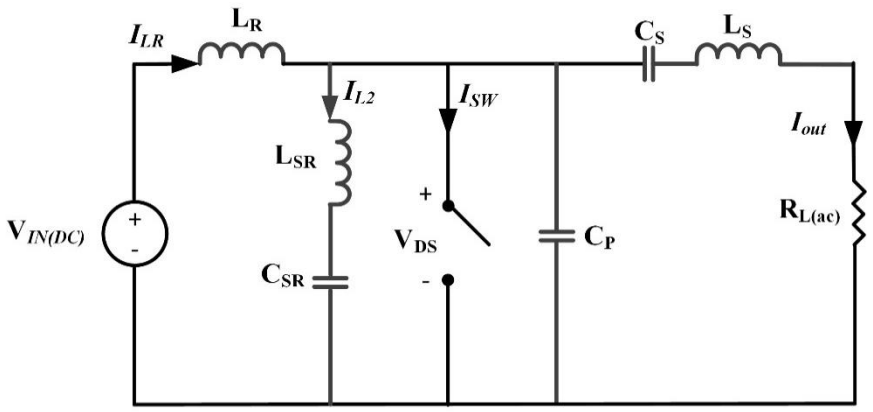

Figure 3.4: Circuit diagram of voltage-fed single-switch multi-resonant inverter for analysis.

3.3.1 Circuit Operation

When the switch is ON, the current through the MOSFET is given by equation (3.3). Total switch current can be found by determining i_{L_r}, i_{L_2} , $and\ i_{out}$.

$$i_{sw}(\omega t)_{ON} = i_{L_r}(\omega t)_{ON} - i_{L_2}(\omega t)_{ON} - i_{out}(\omega t)_{ON} \tag{3.3}$$

The current through the input inductor is resonant current and can be defined as equation (3.4) for any duty cycle *D*.

$$i_{L_R}(2\pi D) = 2\pi D \frac{V_{IN}}{\omega L_R} + i_{L_R}(2\pi D)_{OFF} \tag{3.4}$$

The current through the series-tuned second harmonic termination branch (L_{SR} – C_{SR}) can be found using Equation (3.5).

$$i_{L_{SR}}(\omega t) = K_1 \cos(4\pi f t) + K_2 \sin(4\pi f t) \tag{3.5}$$

The coefficients K_1 and K_2 are determined based on the equations boundary conditions. Finally, the output current, i_{out}, can be evaluated as sinusoid using fundamental harmonic approximation (FHA):

$$i_{out}\ (\omega t) = I_m \sin(\omega t + \alpha) \tag{3.6}$$

Where, I_m is the magnitude of output current and "α" is the initial phase between the current and the voltage.

When the switch is OFF, the maximum voltage across the drain to the source port of the MOSFET can be calculated by determining the voltage across capacitor C_P. The parallel capacitor will charge within an arbitrary time and reach a maximum point. The maximum voltage and shape of the drain to source voltage, V_{DS}, will depend on the overall drain-to-source (Z_{ds}) characteristic. The V_{DS} will be a quasi-resonant wave as shown in figure 3.5. The current through C_P based on the duty cycle is given by equation (3.7).

$$i_{C_P}(\omega t)_{OFF} = i_{L_R}(\omega t)_{OFF} - i_{L_2}(\omega t)_{OFF} - i_{out}(\omega t)_{OFF} \tag{3.7}$$

During the OFF condition, the current in the L_{SR}-C_{SR} branch can be determined by applying KCL at drain node,

$$i_{L_2}(\omega t)_{OFF} = i_{L_r}(\omega t)_{OFF} - i_{C_P}(\omega t) - i_{out}(\omega t) \tag{3.8}$$

Equation (3.8) can be written as:

$$i_{L_2}(\omega t)_{OFF} = i_{L_r}(\omega t)_{OFF} - \omega C_P \frac{dV_{DS}}{d\omega t} - I_m \sin(\omega t + \alpha) \tag{3.9}$$

The total voltage across the L_{SR}-C_{SR} branch is (S. Aldhaher et al., 2015):

$$V_{DS}(\omega t) = \omega L_{SR} \frac{di_{L_2}(\omega t)}{d\omega t} + \frac{1}{\omega C_{SR}} \int_{2\pi D}^{\delta} i_{L_2}(\omega t) d\omega t + v_{C_{SR}}(2\pi D) \tag{3.10}$$

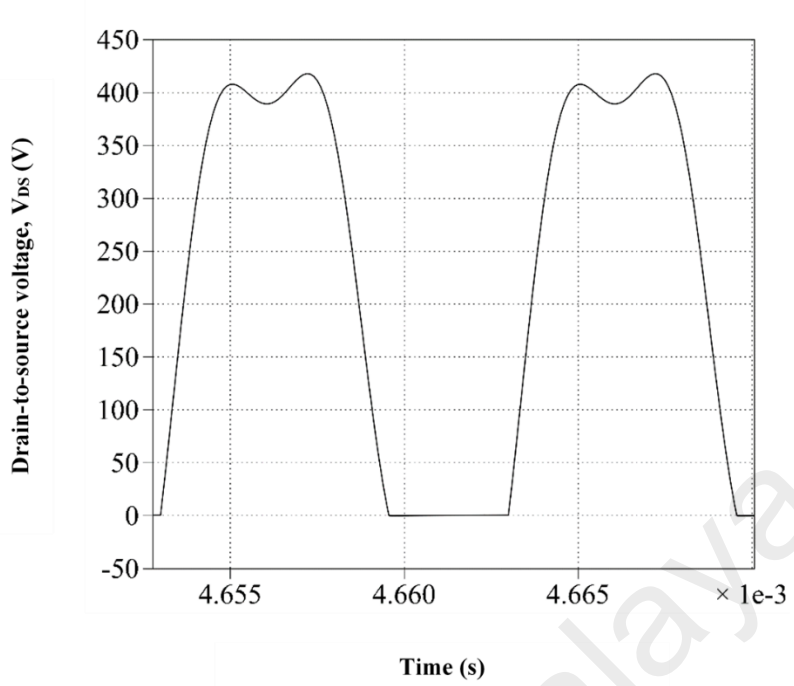

Figure 3.5: The simulated drain-to-source voltage of proposed inverter (Input: 200 V_{DC}).

Differentiating equation (3.10) and substituting $\frac{dV_{DS}(\omega t)}{d\omega t}$ in equation (3.9), the final equation of the current through L_{SR} – C_{SR} branch can be obtained as follows:

$$i_{L_2}(\omega t) = 1 - I_m\, sin(\omega t + \alpha) - \omega^2 L_{SR} C_P \frac{d^2 i_{L_2}(\omega t)}{d\omega t^2} - \frac{C_P}{C_{SR}}\, i_{L_2}(\omega t) \qquad (3.11)$$

The general solution of above (equation 3.11) linear non-homogeneous differential equation is the current through the series resonant branch during OFF condition and it can be given as follows:

$$I_{L_2}(\omega t^-) = K_3 \cos(4\pi f t) + K_4 \sin(4\pi f t) - \frac{m_2^2 n}{m_2^2 - 1} \sin(\omega t + \alpha) + \frac{1}{F+1} \qquad (3.12)$$

Where, $F = \frac{C_P}{C_{SR}}$, $m_2 = 2\sqrt{\frac{F+1}{F}}$ and $n = \frac{1}{F+1} I_m$

K_3 and K_4 values can be determined using the boundary conditions of the equation. The voltage and current continuity condition during switch turn ON and OFF determine the

boundary condition. The current through parallel capacitor can be obtained by using equation (3.10).

$$I_{C_P}(\omega t)_{OFF} = 2\pi D \frac{V_{IN}}{\omega L_R} - n(F+1)\sin(\omega t + \alpha) - I_{L_2}(\omega t)_{OFF} \quad (3.13)$$

The voltage across the C_P, which is the drain to source voltage of the MOSFET is given by (3.14).

$$V_{DS}(\omega t) = \frac{1}{\omega C_P} \int_{2\pi D}^{\omega t = 2\pi} I_{C_P}(\delta) d\delta \quad (3.14)$$

where δ is a constant that indicates the maximum drain to the source voltage slew rate. Equation (9) can be rewritten by incorporating ZVS condition as follows:

$$\frac{1}{\omega C_P} \int_{2\pi D^-}^{2\pi} (2\pi D \frac{V_{IN}}{\omega L_R} - n(F+1)\sin(\omega t + \alpha) - K_3 \cos(4\pi f t) + K_4 \sin(4\pi f t) - \frac{m_2^2 n}{m_2^2 - 1} \sin(\omega t + \alpha) + \frac{1}{F+1}) d\delta = 0 \quad (3.15)$$

MATLAB function "fsolve" can be used to compute the values of unknown variables K_3, K_4, n, and α numerically for specific values of D, m and F. This is one method of calculating the various component of the proposed voltage-fed inverter. However, in this work, a different design technique has been implemented to get the desired result. It has been seen from (3.12), V_{DS} is dependent on m, n, F and D. As "m" and "n" are dependent on F. Therefore, values of F have been deducted first. The peak voltage stress of the semiconductor switch is dependent upon the ratio of "F". It is also seen that, the values of L_S – C_S can be calculated independently. Based on these two insights, the overall new design procedures are described in the following sections.

3.3.2 Derivation of I_m

The switch current can be given as:

$$i_{sw}(\omega t) = 1 - n(F+1)\sin(\omega t + \alpha) - K_1\cos(4\pi f t) + K_2\sin(4\pi f t) \quad (3.16)$$

The average switch current is equal to DC input current (S. Aldhaher et al., 2015), hence,

$$\frac{1}{2\pi}\int_0^{2\pi} i_{sw}(\omega t)d(\omega t) = 1$$

$$= \frac{n}{2\pi}(\cos(2\pi D + \alpha) - \cos\alpha)(F+1) + D - \frac{1}{4\pi f t}(K_1\sin(4\pi f t D) + 2K_2\sin^2(4\pi f t D)) \quad (3.17)$$

Solving (3.17) we have,

$$n = \frac{2\pi(1-D) + (K_1\sin(4\pi f t D) + 2K_2\sin^2(4\pi f t D)}{(F+1)(\cos(2\pi D + \alpha) - \cos\alpha)} \quad (3.18)$$

As $n = \frac{1}{F+1}I_m$, substituting (3.18) into this equation

$$I_m = \frac{2\pi(1-D) + (K_1\sin(4\pi f t D) + 2K_2\sin^2(4\pi f t D)}{\cos(2\pi D + \alpha) - \cos\alpha} \quad (3.19)$$

3.3.3 Design Procedure

3.3.3.1 Calculation of L_S – C_S and C_P

The values of L_S can be computed according to the specific application requirement. In this work, L_S is the inductance of the primary coil of a loosely coupled transformer. These types of transformers are widely used in IPT application. In the case of IPT system, a reflected impedance is also added with L_S.

C_S is calculated such that the resonance frequency of $L_S - C_S$ becomes lower than switching frequency. A proper selection of this frequency is necessary for maintaining proper voltage gain. The combined effect of $L_S - C_S$ contributes in the reduction of the switch voltage stress.

Value of C_P is calculated to maintain the ZVS operation of MOSFET. The following criteria must be met while calculating the value of C_P.

$$f_{L_s-C_S} < f_s \leq f_{L_S-(C_S||C_P)} \tag{3.20}$$

Here, f_S, is the switching frequency. $f_{L_s-C_S}$ and $f_{L_S-(C_S||C_P)}$ is given by:

$$f_{L_s-C_S} = \frac{1}{2\pi\sqrt{L_s C_s}}$$

$$\text{and } f_{L_S-(C_S||C_P)} = \frac{1}{2\pi\sqrt{L_S C_S C_P/(C_S+ C_P)}} \tag{3.21}$$

After calculating the value of C_P, the value of C_{SR} is determined from the value of F. Different values of F will cause a different level of voltage and current stress on semiconductor switch. In figure 3.6, based on various F, a family of curves has been given for duty cycle vs V_{DS}. The x-axis represents the duty cycle and y-axis the peak switch voltage stress (multiple of input DC voltage). It is seen from the curves that when F values lie between 1.2 – 1.4, V_{DS}, becomes less within the duty cycle range 30-40%. Peak voltage stress increases rapidly with duty cycle after a threshold and ZVS cannot be maintained.

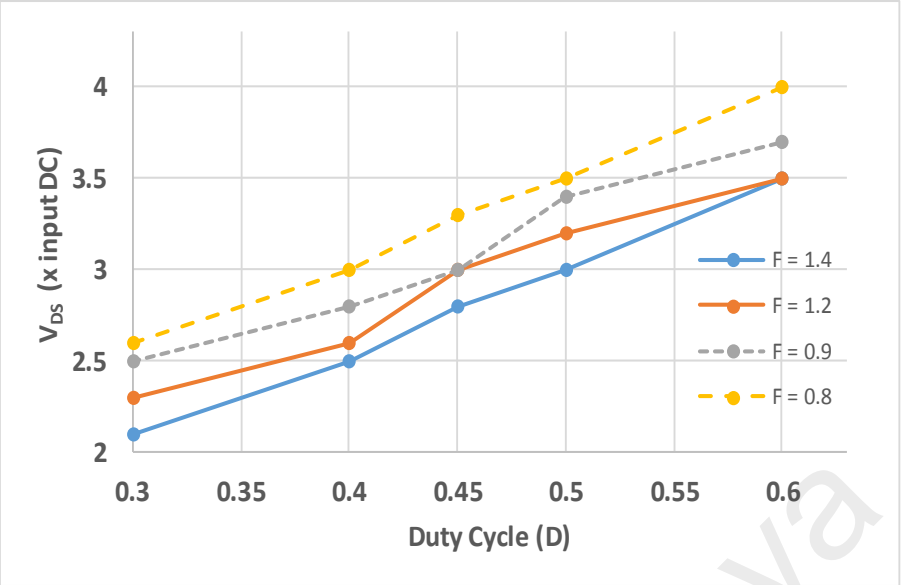

Figure 3.6: Duty cycle vs V_{DS} for different F values.

3.3.3.2 Values of L_R, L_{SR} – C_{SR}

Once F and C_P are calculated, C_{SR} can be calculated using equation $F = \frac{C_P}{C_{SR}}$. L_{SR} is calculated such that, it resonates with C_{SR} on the second harmonic of the switching frequency. Using (3.22), the value of L_{SR} can be calculated. Equation (3.23) shows that, the resonance frequency of L_R and C_P will be slightly above the switching frequency. Once C_P is determined, then, L_R is calculated by (3.23). It is seen that, the resonant frequency of L_R and C_P, could work as design criteria of the inverter. This resonant frequency is chosen such that, ZVS of the MOSFET can be achieved up to 60% of load change.

$$L_{SR} = \frac{1}{16\pi^2 f_s^2 C_{SR}} \tag{3.22}$$

$$f_{L_R-C_P}\left(= \frac{1}{2\pi\sqrt{L_R C_P}}\right) > f_S \tag{3.23}$$

In summary, overall design procedure can be described as follows:

- Calculate L_S according to the application specification

- C_S and C_P are determined according to the condition specified in (3.20) and (3.21)
- Based on C_P and F, C_{SR} is calculated
- L_{SR} is calculated by (3.22)
- The value of L_R is found based on equation (3.23)

3.4 Summary

The detail mathematical modelling and calculation of various component values of proposed inverter have been shown in this chapter. Analytical equations have been derived to find the voltage and current of various components. The component values have been calculated to maintain a proper drain-to-source impedance. This same procedure can be used for designing the proposed inverter with much higher frequency range IPT applications. Using this design procedure ZVS of the MOSFET could be maintained even at coil misalignments of 30%.

CHAPTER 4: SIMULATION AND EXPERIMENTAL RESULT

4.1 Introduction

Simulation model and result will be analyzed in this chapter. After that, prototype implementation and experiment result will be discussed to verify the theory presented in chapter 3.

4.2 Simulation Model

To verify the design concept, a simulation model of the proposed voltage source multi-resonant inverter with an IPT system has been built using MATLAB/SimPowerSystem toolbox.

The schematic diagram of the complete system and simulation model have been shown in figure 4.1 and 4.2 respectively. It is designed to transfer 1 kW power across a vertical gap distance of 8 cm. Primary inductance, secondary inductance, and mutual inductance have been measured using an LCR meter with 8 cm vertical gap and up to 30% horizontal misalignment (Hayes, Donovan, Egan, & Donnell, 2003). Then these inductances are inserted into the simulation model. The rest of the inverter components are calculated using the method described in above section. The primary or transmitter side forms a *capacitor-inductor-capacitor (CLC)* compensation as shown in figure 4.1. Series compensation has been used in the secondary or vehicle side of the system.

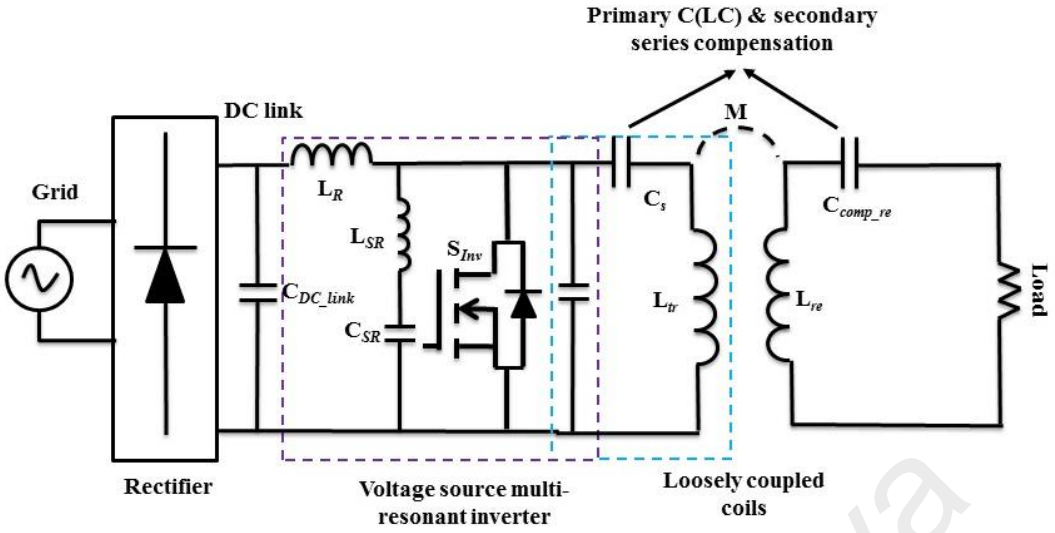

Figure 4.1: IPT system configuration schematic with the proposed inverter.

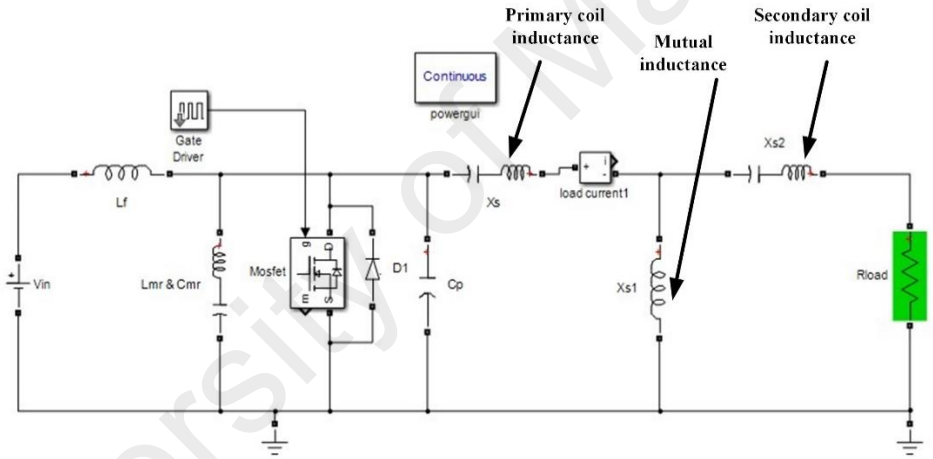

Figure 4.2: Simulation Model.

Value of C_S is obtained by setting the resonance frequency of L_S-C_S to 95 kHz according to (3.20). The switching frequency in this work is selected as 100 kHz. Using C_S value, C_P is obtained again using (3.20). From the curve of figure 3.6, "F" value is chosen between 1.4-1.5 range.

Then, C_{SR} is calculated according to $F = \frac{C_P}{C_{SR}}$ and subsequent other component values have been found using consecutive steps described in above section. Duty cycle has been kept at 30% all the time according to figure 3.6. The values of L_R, C_{SR}, C_P and C_S have

been changed for further tuning during simulation to get the final inverter model. The inverter maintains ZVS even in considerable load changes (60%). It provides good power output with reduced switch voltage stress. The peak voltage stress is reduced considerably compare to other single switch inverters (Aldhaher, Luk, et al., 2014b; S. Aldhaher et al., 2015; Aldhaher et al., 2016).

It is seen from the simulation result that peak voltage only reaches up to 2 times of input DC voltage. Whereas, for other single switch inverter, this peak voltage stress goes up to 2.5-3.5 times with same output power transfer capability. Besides, the proposed inverter has all the inherent advantages of class E-type inverter. Final component values of the simulated model have been listed in Table 4.1.

Table 4.1: Simulation Parameters

Components	Values
L_R	15 µH
L_{SR}	6.5 µH
C_{SR}	100 nF
C_S	26 nF
C_P	146 nF
Inductance of primary coil of IPT system, L_S	100.38 µH
Inductance of secondary coil of IPT system	103.77 µH
Secondary side compensation capacitor	24.5 nF
Mutual inductance	14.85 µH
Load resistance	25 Ω
Duty cycle	30%
$f_{L_s-C_S}$	98.517 kHz
$f_{L_R-C_P}$	107.55 kHz
$f_{L_S-(C_S\|\|C_P)}$	107.1 kHz
Voltage and Power rating	200 V and 1 kW

4.3 Simulation Result and Discussion

In figure 4.3(a), drain-source voltage (V_{DS}) and current (I_{DS}) waveform of the proposed inverter have been shown. V_{DS} has maintained ZVS/ZDS at turn-on. It also provided less peak stress as calculated theoretically by using figure 3.6. Given 200V DC input voltage, the peak stress across the switch is 400V. However, I_{DS} is a little bit higher in the simulation. This is due to the simulation method used in Simulink/SimPowerSystem toolbox. This problem may be solved by developing a custom component model of the

inductor, capacitor etc. This is beyond the scope of this work. Thus, existing component models have been used.

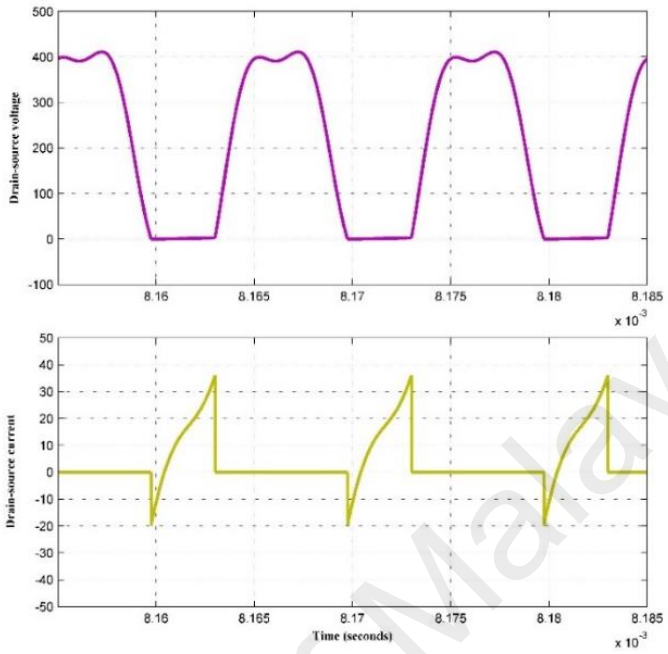

(a)

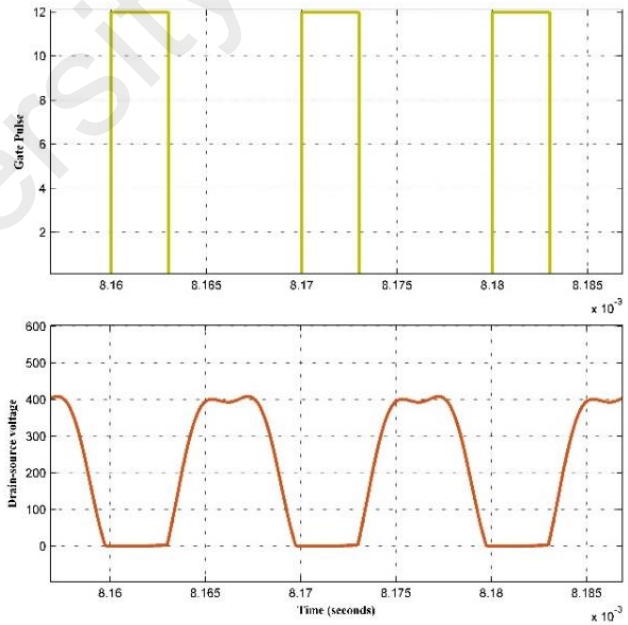

(b)

Figure 4.3: (a) V_{DS} and I_{DS} at full load (DC Input: 200V) (b) V_{GS} and V_{DS}

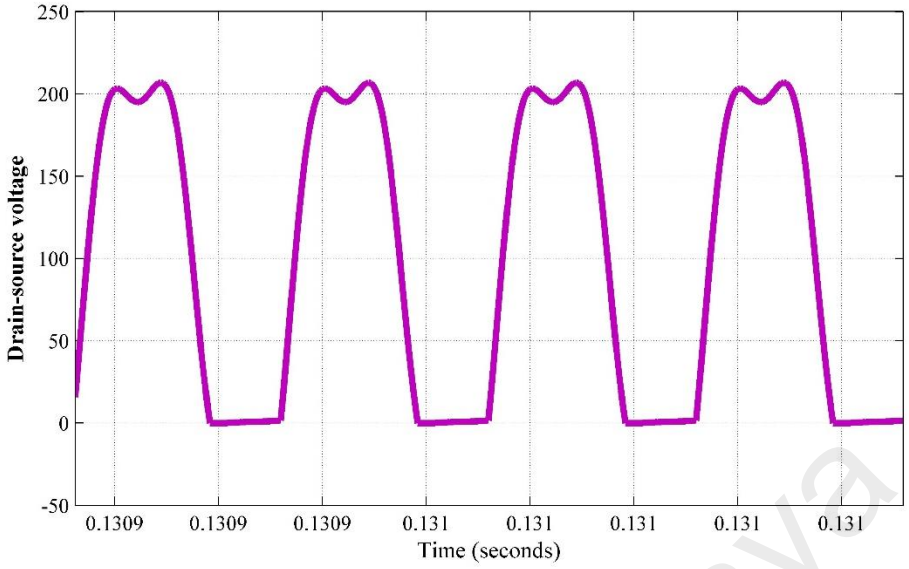

Figure 4.4: V_{DS} at full load with 200V DC Input

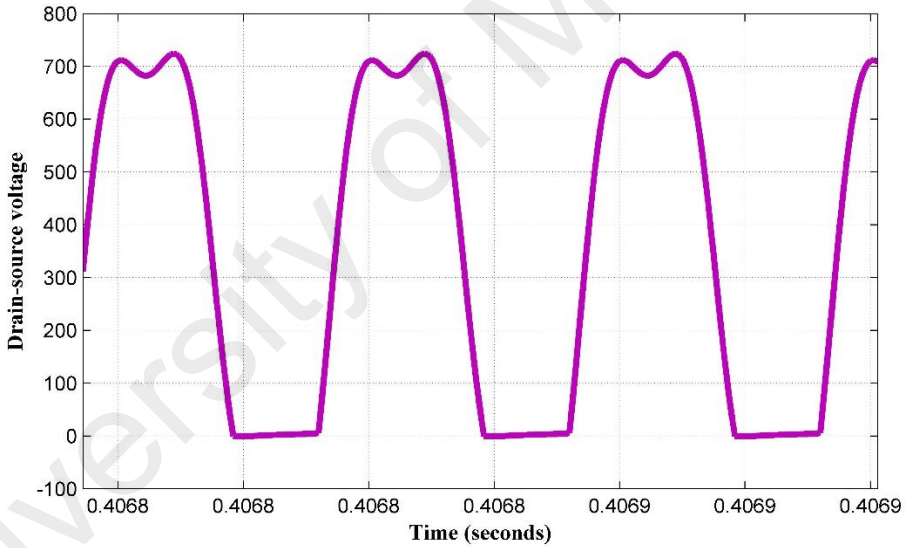

Figure 4.5: V_{DS} at full load with 350V DC Input

The voltage stress across MOSFET during 100 V DC input and 350 V DC input has been depicted in Figure 4.4 and 4.5. It also maintains the theoretical characteristics as mentioned earlier.

This inverter shows good operating characteristics during considerable load changes as depicted in figure 4.6. DC equivalent ac resistance is used for both practical and simulation purposes to observe the load voltage and current. Load voltage and current

waveform have been given in figure 4.7(a). Voltage and current both are in phase and resonance, indicating efficient power transfer. Drain to source impedance (Z_{DS}) characteristic curve shown in figure 4.7(b) depicts the magnitude and phase at 100 kHz operating frequency. It has been observed that, to maintain ZVS and reduce peak switch stress it is necessary to maintain a certain Z_{DS} magnitude and phase. Figure 4.7(b) shows the chosen operating point for this design. Some other operating points could also be chosen if impedance magnitude and phase do not come below 20Ω and 23°.

It is observed that below these limits of impedance magnitude and phase, the proposed inverter could not maintain efficient operation due to hard switching. The overall system has constant output voltage characteristics with load change as shown in figure 4.8.

Inverter efficiency is calculated by subtracting the losses of L_R, $L_{SR} - C_{SR}$ branch, switch conduction loss, off time loss, loss through C_P, and so on. This detailed simulation model is used to build the experiment setup. The details experimental result and discussion are provided in the following section.

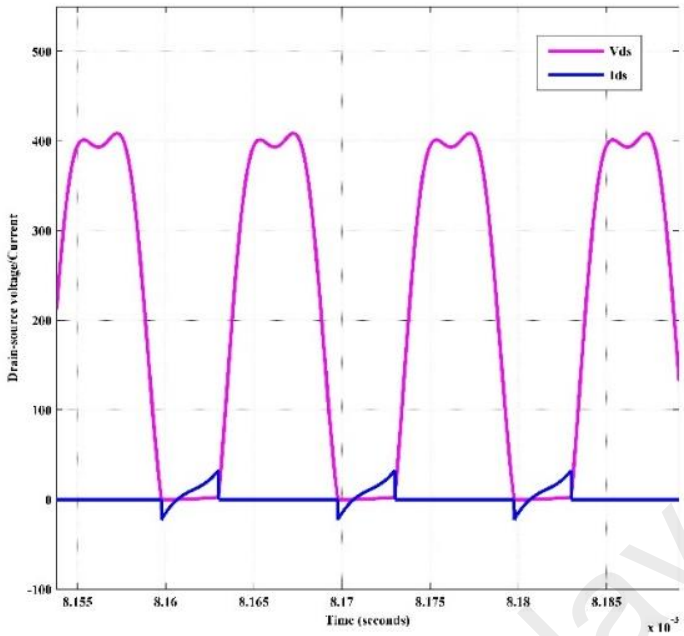

(a)

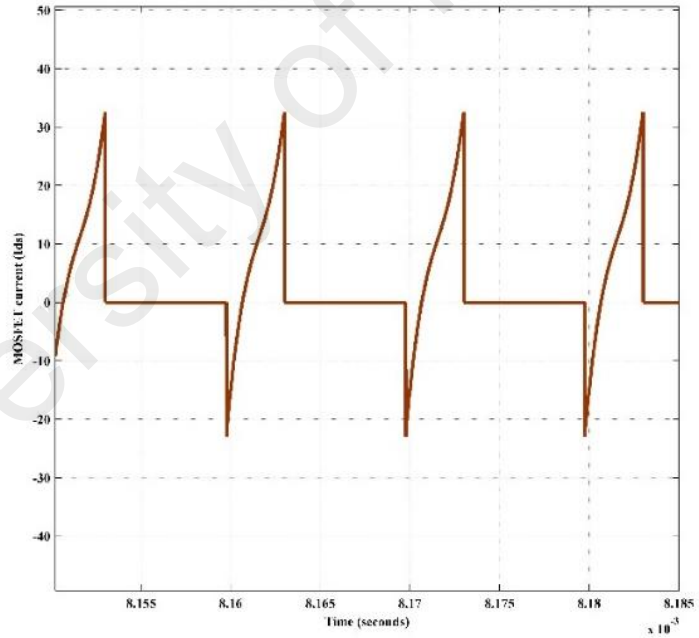

(b)

Figure 4.6: (a) V_{DS} and I_{DS} (Vertical Axis) at 40% load change with respect to time (seconds, Horizontal Axis) at 200V DC (b) I_{DS} (magnified, Vertical Axis).

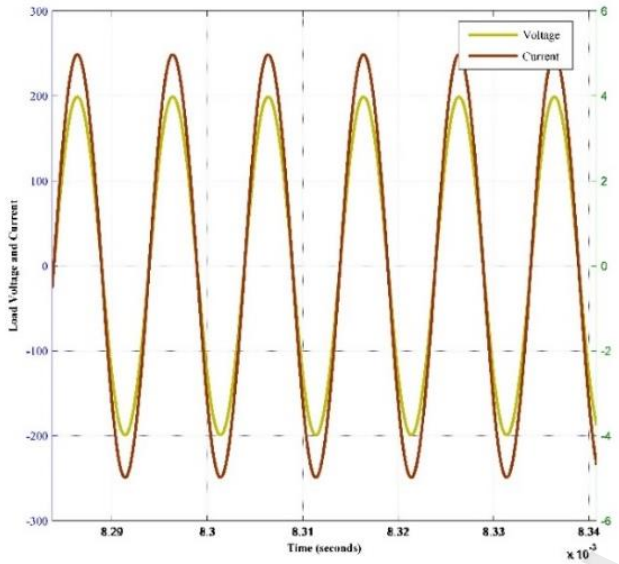

(a)

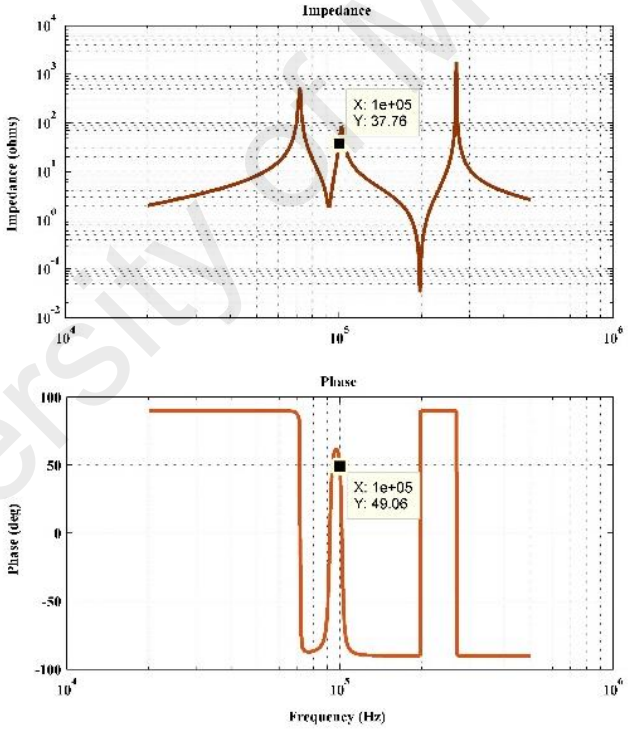

(b)

Figure 4.7: (a) Load voltage and current (b) Drain-source impedance magnitude and phase.

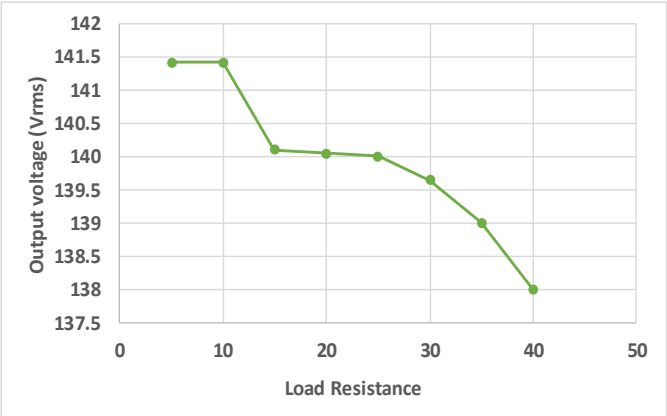

Figure 4.8: Output voltage vs Load resistance (Input DC: 200V).

4.4 Description of Prototype

A 500W experiment setup was built as shown in figure 4.7 to verify the operation and performance of the proposed voltage source multi-resonant inverter with WPT system. The specifications of the prototype are listed in Table 4.2. Due to the limitation of proper electromagnetic shielding and to maintain the safety of digital controller, maximum 150 W has been transferred to measure the efficiency and other parameters.

The gate signal was generated using an ePWM module of Texas Instruments TMS320F28335 digital signal processor. Experiment results are given in figure 4.8-4.10.

4.5 Experiment Result and Discussion

V_{DS} and V_{GS} completely agree with the simulation result. V_{DS} has the exact voltage wave-shape and peak stress as designed. V_{DS} has a spike during turn-off instant. This is due to the mismatch between gate-to-source and gate driver output impedance. This can be mitigated by modifying the gate driver circuit design. In the current gate driver, the output impedance is controlled using a fixed resistor. However, by introducing a variable resistor the output impedance of the gate drive circuit can be varied to match the gate-source impedance of the MOSFET. This will eliminate unwanted ringing during turn-off condition which in turns reduces the spike of V_{DS}. Primary side voltage and current are not in resonance because of the multi-resonance characteristic in the primary side.

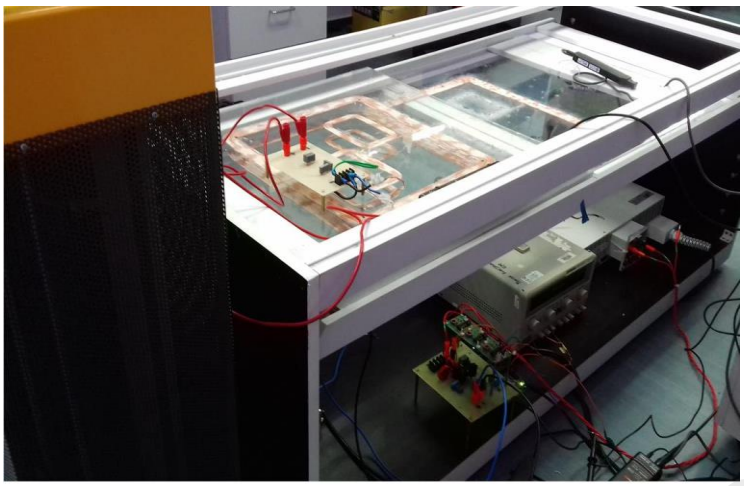

(a)

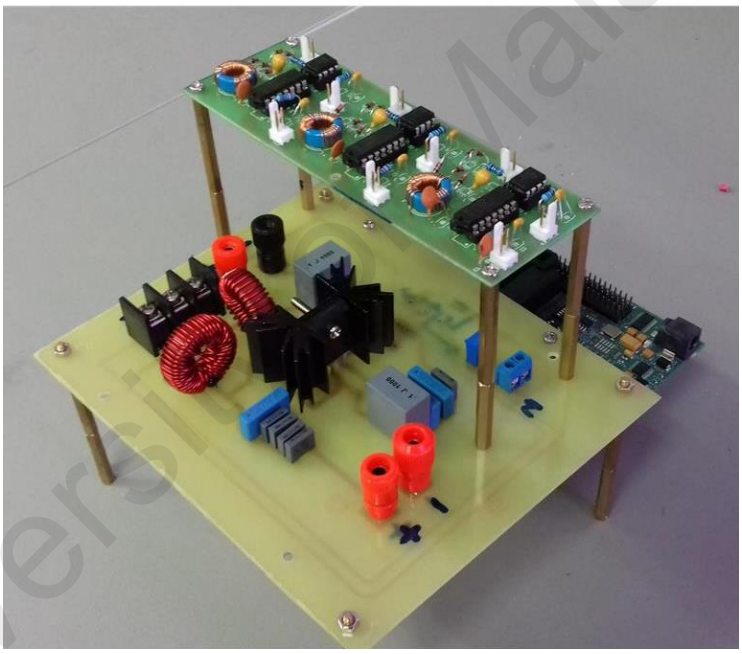

(b)

Figure 4.9: (a) Complete experiment setup (b) Proposed single switch inverter prototype.

Table 4.2: Specifications of the Prototype

Inverter components	**Value**	**Manufacturer**
L_R	14 µH – 15 µH	Coilcraft
L_{SR}	6.5 µH	Coilcraft
C_{SR}	98.55 nF (Polypropylene)	KEMET
C_P	146 nF (Polypropylene)	KEMET
C_S	26 nF (Polypropylene)	KEMET
C_{sec_comp}	25.2 nF (Polypropylene)	KEMET
MOSFET	CREE C2M0080120D SiC MOSFET (V_{DS} = 1200 V, I_D = 36 A at 25 °C	
DSP (for inverter control)	Texas Instrument TMS320F28335 eZDSP board and gate driver circuit	
Coil parameters	**$L_{Primary}$**	**$L_{Secondary}$**
	100.38 µH	103.77 µH
Total power	500 W (150 W used in the experiment)	
Input Voltage	100- 130V	

Load voltage and current have a small phase shift. This phenomenon occurs due to the out-of-resonance operation of the secondary side. It mainly happens due to the high leakage magnetic field of the IPT coils. It could be reduced by proper design of the coil.

This phase-shift increases and affects the power transfer efficiency during misalignment condition.

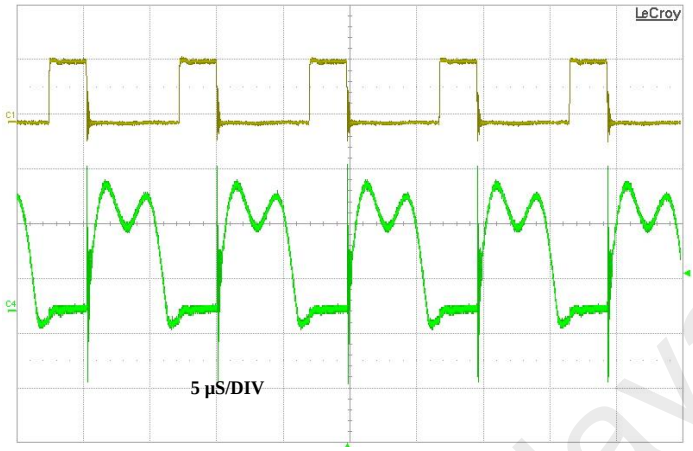

(a)

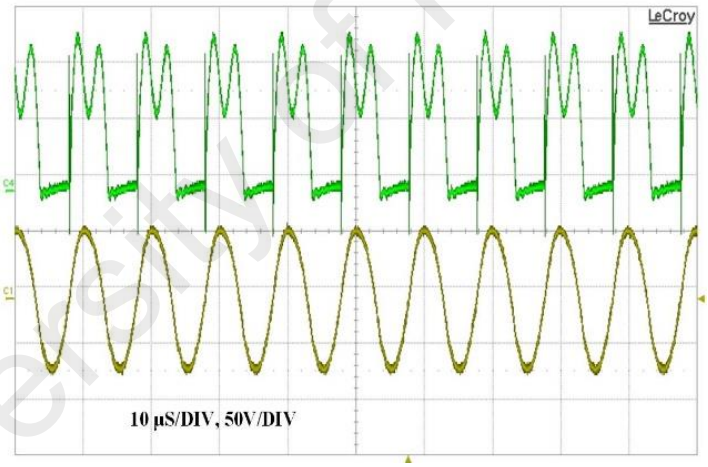

(b)

Figure 4.10: (a) V_{GS} and V_{DS} (b) V_{DS} and Load voltage.

Figure 4.11(a) shows that primary and secondary side voltages are in phase, indicating proper magnetic coupling. Figure 4.11(b) shows the V_{DS} recorded at 30% misalignment. The peak voltage stress could be maintained at 30% misalignment condition of IPT coils. This feature is important for primary side inverters used in IPT system.

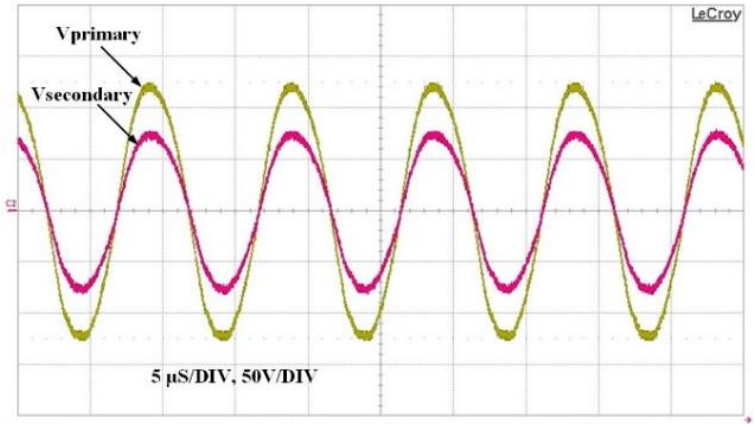

(a)

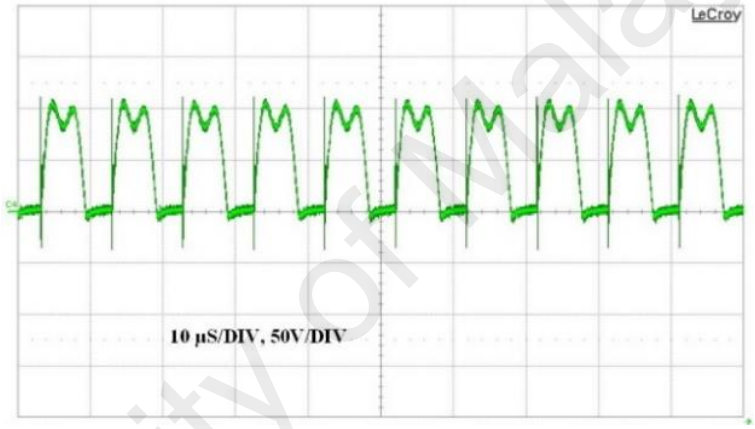

(b)

Figure 4.11: (a) Primary side voltage and secondary side voltage (b) Peak V_{DS} at 30% misalignment condition (Input voltage: 50V DC).

A performance evaluation of the proposed inverter with two class E and class EF_2 high- frequency resonant inverter topologies, as shown in Table 4.3. In every category, the proposed inverter has demonstrated better operating characteristics. The drain-to-source voltage across MOSFET in the proposed inverter is less than that of the conventional class EF_2 inverter. L_R is a resonant inductor in the proposed topology that reduces losses and size. Thus, the system can be designed to become compact and power density could be increased. The constant voltage characteristics could be maintained (Figure 4.6), which is desirable for IPT application. Besides, these inverters have the

inherent sine-wave characteristics (Figure 4.12) like those of conventional class EF_2 and class E inverter. The proposed modified class EF_2 inverter can deliver similar output power with less device stress and losses than its conventional counterpart.

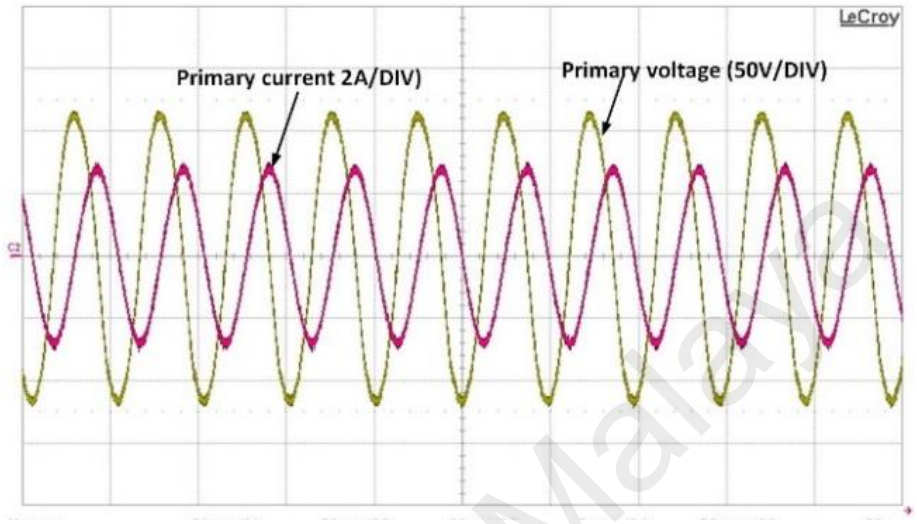

(a)

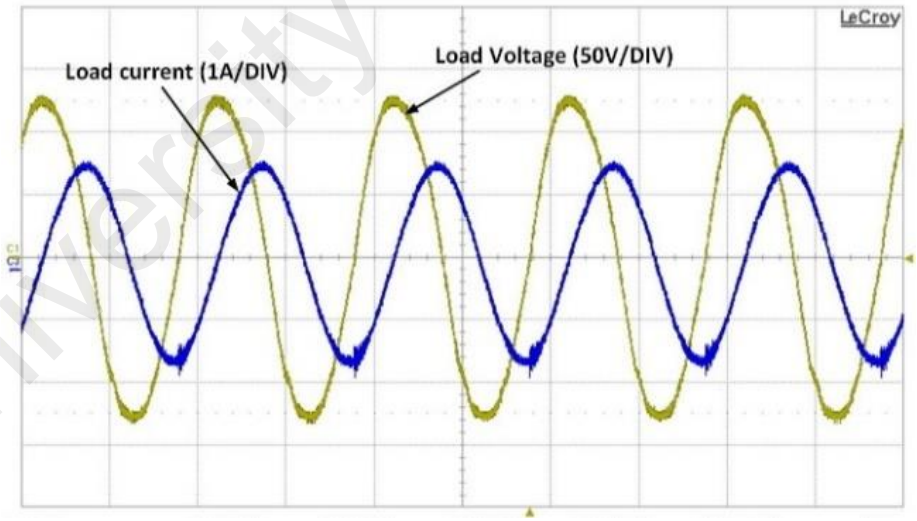

(b)

Figure 4.12: (a) Primary voltage and current (b) Secondary voltage and current.

Table 4.3: Performance Evaluation of Proposed Modified Voltage-Fed Multi-Resonant Class EF_2 Inverter with Class E and Conventional Class EF_2 Inverters

Parameters	Class E (Aldhaher, Luk, Bati, & Whidborne, 2014; Aldhaher, Luk, et al., 2014b; Kazimierczuk & Czarkowski, 2012; Phinney et al., 2007; Pinuela et al., 2013; Rivas, Han, Leitermann, Sagneri, & Perreault, 2007; Sokal & Sokal, 1975)	Class EF_2 (Samer Aldhaher et al., 2015; S. Aldhaher et al., 2015; Aldhaher et al., 2016; Kaczmarczyk, 2006; Kee et al., 2003; Rivas et al., 2007)	**Modified class EF_2 (Our work)**
Generic			
V_{DS} (V) (times input DC)	3.5	2.5	2
Input DC voltage (V)	100–200	100–200	100–350
Output voltage and current	Sinusoidal	Sinusoidal	Sinusoidal
Input inductor current	Constant	Constant	Resonant (variable)
Input inductor loss	High	High	Low
Circulating current	-	-	Low
ZVS	Dependent on the load impedance	Dependent on the load impedance	Less dependent on the load impedance
ZDVS (zero derivative switching)	Maintained	Maintained	Maintained
ZCS	Hard to maintain	Partially maintained	Partially maintained
Efficient operation at frequency range	500 kHz – 6.8 MHz	1 MHz – 13.6 MHz	100 kHz – 30 MHz
With IPT system			
Misalignment tolerance	-	-	High
Change in drain-to-source voltage	Hard to keep within SOA of MOSFET during misalignment condition (10-20%)	Hard to keep within SOA of MOSFET during misalignment condition (10-20%)	Can be kept within SOA of MOSFET up to 30% misalignment of IPT coils
Integration with IPT system	Difficult to integrate with IPT system	Difficult to integrate with IPT systems which operate on less than 200 kHz	Easier integration even with IPT systems which operate on frequency range less than 200 kHz
Tuning procedure	Tuning different components in conjunction with IPT system is difficult	Tuning procedure is complex while integrating with IPT system	Tuning procedure is simple for IPT system
Efficiency	90%	88%	90%±2 (perfectly aligned condition)

Figure 4.13(a) and (b) show the efficiency of the inverter for two types of misalignment condition. Figure 4.14(a) and (b) shows the coupling variations of the WPT coil used for this experiment. Efficiency during vertical misalignment is lower than in horizontal misalignment because of the low coupling and high leakage magnetic field of the coils. This efficiency measurement was conducted during 150-W power transfer condition. Power transfer was maintained in this range because of some experimental limitation. At this operating condition, the losses in L_R, $L_{SR} - C_{SR}$ branches, switch conduction, off time loss, and loss through C_P were calculated using Equations (4.1) to (4.4).

The loss in the input resonant inductor is equal to

$$P_{L_R} = (I^2_{L_R(rms)}) r_{L_R}\,, \tag{4.1}$$

where r_{L_R} is the ESR of the resonant inductor measured by the LCR meter.

The switch conduction loss is calculated using (4.2) with switch rms current and on-time resistance $r_{DS}(ON)$.

$$P_{cond} = I^2_{S(rms)} r_{DS} = [\left(\sqrt{\frac{1}{2\pi}\int_0^{2\pi D} i_s^2 d(\omega t)}\right)] r_{DS}. \tag{4.2}$$

The power loss in C_P due to ESR r_{C_P} is calculated by (4.3)

$$P_{C_P} = [(\sqrt{\frac{1}{2\pi}\int_{2\pi D}^{2\pi} (i_{C_p})^2\, d(\omega t)})] r_{C_P}\,, \tag{4.3}$$

and the total power loss in L_{SR}-C_{SR} is

$$P_{L_{SR}-C_{SR}} = I^2_{L_{SR}(rms)} (r_{L_{SR}} + r_{C_{SR}}) \tag{4.4}$$

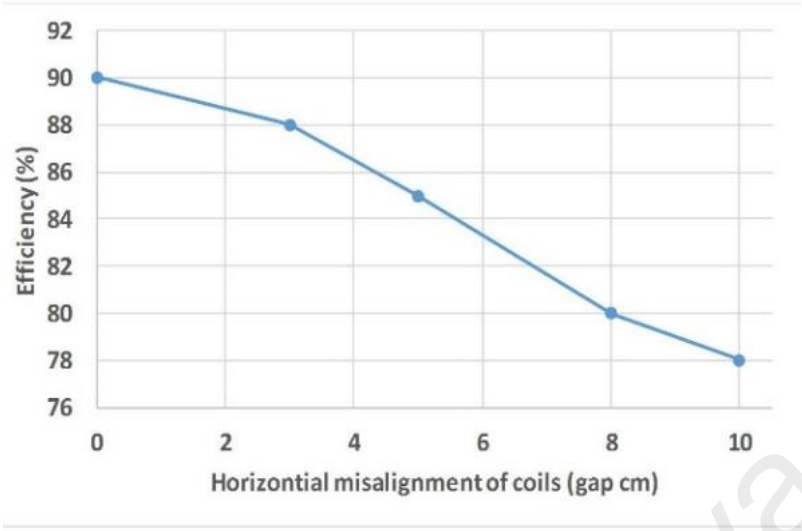

(a)

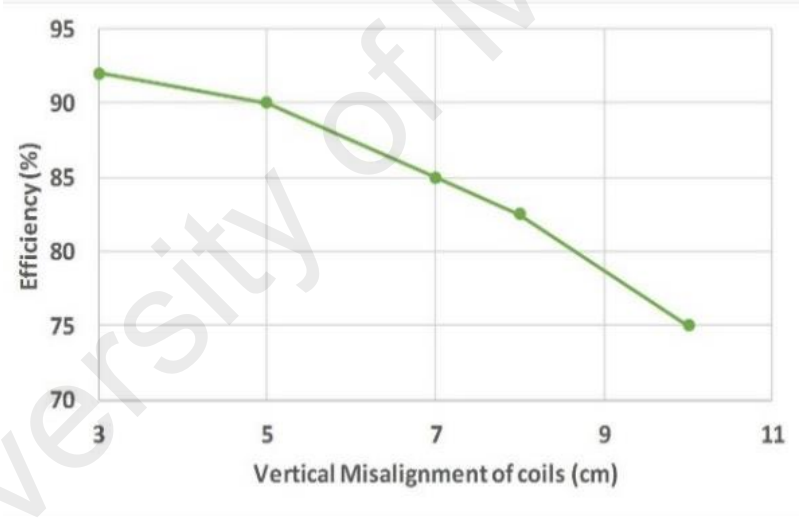

(b)

Figure 4.13: Inverter efficiency (a) during horizontal misalignment, (b) during vertical misalignment.

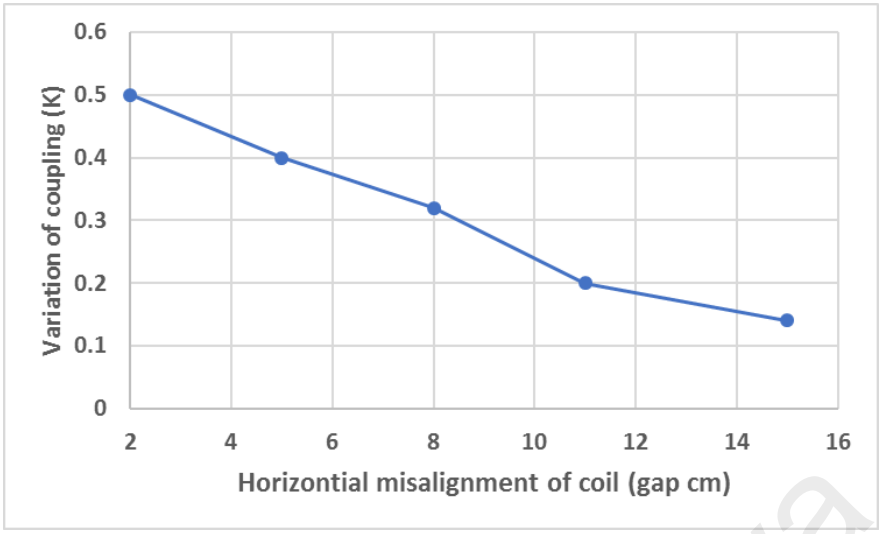

(a)

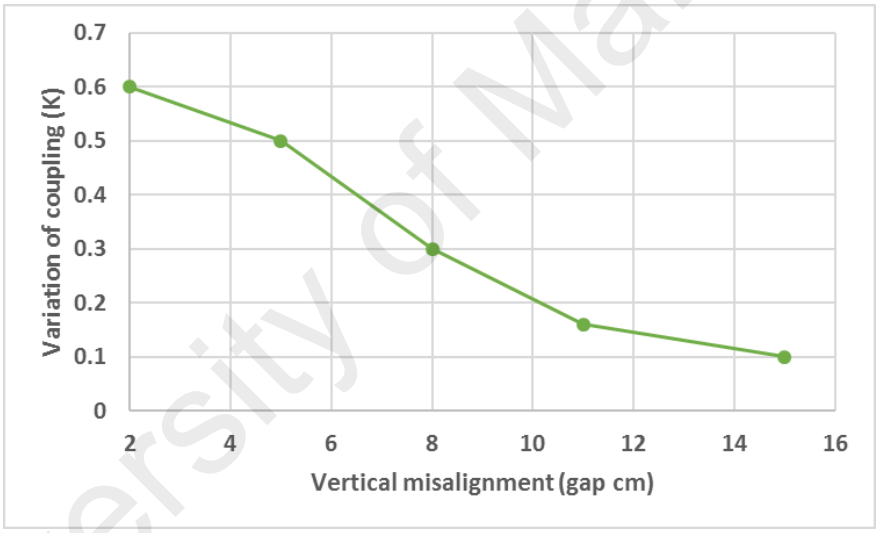

(b)

Figure 4.14: Changes of coupling coefficient (a) during horizontal misalignment, (b) during vertical misalignment.

4.6 Summary

This chapter explains the simulation model and hardware realization of the proposed voltage-fed modified class EF_2 inverter. Simulation and experimental results have been explained. The inverter exhibits excellent performance with IPT system. It can maintain less voltage and current stress and deliver higher power. It works well during considerable misalignment condition of the IPT system and maintains ZVS. Comparison of the proposed inverter with class E and convention class EF_2 inverter shows considerable improvement in terms of efficiency, switching device stress and reliability.

CHAPTER 5: CONCLUSION

5.1 Introduction

The conclusion of the research work is presented in this paper. The key contributions and their impact are described. Finally, some significant future work and application area have been highlighted.

5.2 Conclusion

A modified class EF_2 inverter and its application in IPT system have been presented in this study. The inverter has been designed, developed and analyzed for an IPT vehicle charging system. A pre-built IPT transformer (loosely coupled transformer)/coils has been used. The focus of this study is to design an IPT EV charging system which can be integrated with any type of vehicle side charge controller circuit.

In the proposed inverter, some significant modifications have been made compared to conventional class EF_2 and class E inverters. An input resonant inductor has been used instead of bulky choke inductor. Consequently, loss in the inductor is reduced. This resonant inductor also works in conjunction with a passive resonant circuit to maintain some specific impedance profile which reduces switching device stress. Using a passive resonant circuit, peak voltage stress across the switching device is reduced considerably. The proposed inverter can maintain constant voltage characteristic up-to 30% misalignment of primary and vehicle side coil. The switch operates under zero voltage switching condition and with reduced voltage stress across it. Furthermore, all the inherent advantages of single-switch class E inverter are maintained.

An intuitive design method was described to calculate the various component values of the proposed inverter for an IPT system. The inverter is experimentally verified using a 500-W IPT setup with a frequency range of 95 kHz–100 kHz. The maximum efficiency of the inverter is 90%±2 and maintains good operation during misaligned conditions of

the IPT system. Through the same design procedure, the component value of the proposed inverter can be calculated for other IPT applications.

5.3 Future Work

Based on the observation and findings during this study, the following topics are suggested as future research areas:

1. The tuning used in this work has been calculated manually. However, the procedure can be automated and using auto-tuning voltage stress and efficiency of the inverter can be controlled up to 40-50% misalignment of IPT coils. Thus, automatic tuning may be implemented on the proposed system.
2. The increase of frequency beyond 85 kHz expected to have beneficial effects on the system performance and overall compactness of the IPT system. Evaluation of higher frequency IPT system with the proposed inverter could be aimed for future research work.
3. Vehicle side power electronics DC-DC converter can be added to observe the overall system performance.

REFERENCES

Aldhaher, S. (2014b). *Design And Optimization Of Switched-Mode Circuits For Inductive Links* (Doctoral Dissertations). Retrieved from https://dspace.lib.cranfield.ac.uk

Aldhaher, S., Kkelis, G., Yates, D. C., & Mitcheson, P. D. (2015). Class EF_2 inverters for wireless power transfer applications. *Paper presented at the IEEE Wireless Power Transfer Conference (WPTC)*, 1-4.

Aldhaher, S., Luk, P. C. K., Bati, A., & Whidborne, J. F. (2014). Wireless Power Transfer Using Class E Inverter With Saturable DC-Feed Inductor. *IEEE Transactions on Industry Applications, 50*(4), 2710-2718.

Aldhaher, S., Luk, P. C. K., & Whidborne, J. F. (2014a). Electronic Tuning of Misaligned Coils in Wireless Power Transfer Systems. *IEEE Transactions on Power Electronics, 29*(11), 5975-5982.

Aldhaher, S., Luk, P. C. K., & Whidborne, J. F. (2014b). Tuning Class E Inverters Applied in Inductive Links Using Saturable Reactors. *IEEE Transactions on Power Electronics, 29*(6), 2969-2978.

Aldhaher, S., Yates, D. C., & Mitcheson, P. D. (2015). Modelling and Analysis of Class EF and Class E/F Inverters with series-tuned resonant networks. *IEEE Transactions on Power Electronics, PP*(99), 1-1.

Aldhaher, S., Yates, D. C., & Mitcheson, P. D. (2016). Design and Development of a Class EF_2 Inverter and Rectifier for Multi-megahertz Wireless Power Transfer Systems. *IEEE Transactions on Power Electronics, PP*(99), 1-1.

Atabani, A., Badruddin, I. A., Mekhilef, S., & Silitonga, A. (2011). A review on global fuel economy standards, labels and technologies in the transportation sector. *Renewable and Sustainable Energy Reviews, 15*(9), 4586-4610.

Bosshard, R. (2015). *Multi-Objective Optimization of Inductive Power Transfer Systems for EV Charging* (Doctoral Dissertations). Retrieved from https://www.pes.ee.ethz.ch

Bosshard, R., Badstubner, U., Kolar, J. W., & Stevanovic, I. (2012). Comparative evaluation of control methods for Inductive Power Transfer. *Proceedings of the International Conference on Renewable Energy Research and Applications*.

Bosshard, R., & Kolar, J. W. (2016). Multi-Objective Optimization of 50 kW/85 kHz IPT System for Public Transport. *IEEE Journal of Emerging and Selected Topics in Power Electronics, 4*(4), 1370-1382.

Bosshard, R., Kolar, J. W., Muhlethaler, J., Stevanovic, I., Wunsch, B., & Canales, F. (2015). Modeling and η-α-Pareto Optimization of Inductive Power Transfer Coils for Electric Vehicles. *IEEE Journal of Emerging and Selected Topics in Power Electronics, 3*(1), 50-64.

Bosshard, R., Kolar, J. W., & Wunsch, B. (2014). Control Method for Inductive Power Transfer with High Partial-Load Efficiency and Resonance Tracking. *Paper presented at the 2014 International Power Electronics Conference*.

Ching, T. W., & Chan, K. U. (2008). Review of soft-switching techniques for high-frequency switched-mode power converters. *Paper presented at the IEE Vehicle Power and Propulsion Conference*.

Diekhans, T., & De Doncker, R. W. (2015). A Dual-Side Controlled Inductive Power Transfer System Optimized for Large Coupling Factor Variations and Partial Load. *IEEE Transactions on Power Electronics, 30*(11), 6320-6328.

Esteban, B., Sid-Ahmed, M., & Kar, N. C. (2015). A Comparative Study of Power Supply Architectures in Wireless EV Charging Systems. *IEEE Transactions on Power Electronics, 30*(11), 6408-6422.

Fukuoka, H., Iga, Y., Omori, H., Morizane, T., Kimura, N., & Nakaoka, M. (2014). A Novel Type of Wireless V2H System with Bidirectional Resonant Single-Ended Inverter. *Paper presented at the 2014 International Power Electronics Conference*, 3341-3345.

Hao, H., Covic, G. A., & Boys, J. T. (2014). An Approximate Dynamic Model of LCL-T-Based Inductive Power Transfer Power Supplies. *IEEE Transactions on Power Electronics, 29*(10), 5554-5567.

Hayes, J. G., Donovan, N. O., Egan, M. G., & Donnell, T. O. (2003). Inductance characterization of high-leakage transformers. *Paper presented at the IEEE Applied Power Electronics Conference and Exposition*.

Hu, A. P. (2001). *Selected resonant converters for IPT power supplies* (Doctoral Dissertations). Retrived from https://www.researchgate.net

Huang, C. Y., Boys, J. T., & Covic, G. A. (2012). Resonant Network Design Considerations for Variable Coupling Lumped Coil Systems. *Paper presented at the 2012 IEEE Energy Conversion Congress and Exposition*.

Huang, C. Y., James, J. E., & Covic, G. A. (2015). Design Considerations for Variable Coupling Lumped Coil Systems. *Ieee Transactions on Power Electronics, 30*(2), 680-689.

Jia, H., Qianhong, C., Siu-Chung, W., Tse, C. K., & Xinbo, R. (2015). Analysis and Control of Series/Series-Parallel Compensated Resonant Converter for Contactless Power Transfer. *IEEE Journal of Emerging and Selected Topics in Power Electronics, 3*(1), 124-136.

Jiejian, D., & Ludois, D. C. (2015). A Survey of Wireless Power Transfer and a Critical Comparison of Inductive and Capacitive Coupling for Small Gap Applications. *IEEE Transactions on Power Electronics, 30*(11), 6017-6029.

Jin Huh, W. L., Suyong Choi, Gyuhyeong Cho, and Chuntaek Rim. (2013). Frequency-Domain Circuit Model and Analysis of Coupled Magnetic Resonance Systems. *JPE, 13*(2), 275-286.

Jungwon, C., Tsukiyama, D., Tsuruda, Y., & Rivas, J. (2015). 13.56 MHz 1.3 kW resonant converter with GaN FET for wireless power transfer. *Paper presented at the 2015 IEEE Wireless Power Transfer Conference (WPTC)*.

Kaczmarczyk, Z. (2006). High-Efficiency Class E, EF2 and E/F3 Inverters. *IEEE Transactions on Industrial Electronics, 53*(5), 1584-1593.

Kalwar, K. A., Aamir, M., & Mekhilef, S. (2015). Inductively coupled power transfer (ICPT) for electric vehicle charging – A review. *Renewable and Sustainable Energy Reviews, 47*, 462-475.

Kazimierczuk, M. K., & Czarkowski, D. (2012). *Resonant power converters* (2nd ed.). Hoboken, New Jersey: John Wiley & Sons.

Kee, S. D., Aoki, I., Hajimiri, A., & Rutledge, D. (2003). The class-E/F family of ZVS switching amplifiers. *IEEE Transactions on Microwave Theory and Techniques, 51*(6), 1677-1690.

Kissin, M. L. G., Huang, C. Y., Covic, G. A., & Boys, J. T. (2009). Detection of the Tuned Point of a Fixed-Frequency LCL Resonant Power Supply. *IEEE Transactions on Power Electronics, 24*(3-4), 1140-1143.

Kurs, A., Karalis, A., Moffatt, R., Joannopoulos, J. D., Fisher, P., & Soljačić, M. (2007). Wireless power transfer via strongly coupled magnetic resonances. *Science, 317*(5834), 83-86.

Luk, P. C. K., Aldhaher, S., Fei, W., & Whidborne, J. F. (2015). State-Space Modeling of a Class E^2 Converter for Inductive Links. *IEEE Transactions on Power Electronics, 30*(6), 3242-3251.

Madawala, U. K., & Thrimawithana, D. J. (2012). New technique for inductive power transfer using a single controller. *IET Power Electronics, 5*(2), 248-256.

Mediano, A., & Sokal, N. O. (2013). A Class-E RF Power Amplifier With a Flat-Top Transistor-Voltage Waveform. *IEEE Transactions on Power Electronics, 28*(11), 5215-5221.

Miller, J. M., Onar, O. C., & Chinthavali, M. (2015). Primary-Side Power Flow Control of Wireless Power Transfer for Electric Vehicle Charging. *IEEE Journal of Emerging and Selected Topics in Power Electronics, 3*(1), 147-162.

Nagashima, T., Xiuqin, W., Suetsugu, T., Kazimierczuk, M. K., & Sekiya, H. (2014). Waveform Equations, Output Power, and Power Conversion Efficiency for Class-E Inverter Outside Nominal Operation. *IEEE Transactions on Industrial Electronics, 61*(4), 1799-1810.

Ning, P. Q., Miller, J. M., Onar, O. C., & White, C. P. (2013). A Compact Wireless Charging System for Electric Vehicles. *Paper presented at the 2013 IEEE Energy Conversion Congress and Exposition*.

Onar, O. C., Chinthavali, M., Campbell, S., Ning, P. Q., White, C. P., & Miller, J. M. (2014). A SiC MOSFET Based Inverter for Wireless Power Transfer

Applications. *Paper presented at the 2014 Twenty-Ninth Annual IEEE Applied Power Electronics Conference and Exposition*.

Perreault, D. J., Jingying, H., Rivas, J. M., Yehui, H., Leitermann, O., Pilawa-Podgurski, R. C. N., . . . Sullivan, C. R. (2009). Opportunities and Challenges in Very High Frequency Power Conversion. *Paper presented at the IEEE Applied Power Electronics Conference and Exposition*.

Phinney, J. W., Perreault, D. J., & Lang, J. H. (2007). Radio-Frequency Inverters With Transmission-Line Input Networks. *IEEE Transactions on Power Electronics, 22*(4), 1154-1161.

Pinuela, M., Yates, D. C., Lucyszyn, S., & Mitcheson, P. D. (2013). Maximizing DC-to-Load Efficiency for Inductive Power Transfer. *IEEE Transactions on Power Electronics, 28*(5), 2437-2447.

Qu, X., Jing, Y., Han, H., Wong, S. C., & Tse, C. K. (2017). Higher Order Compensation for Inductive-Power-Transfer Converters With Constant-Voltage or Constant-Current Output Combating Transformer Parameter Constraints. *IEEE Transactions on Power Electronics, 32*(1), 394-405.

Rivas, J. M., Han, Y. H., Leitermann, O., Sagneri, A., & Perreault, D. J. (2007). A high-frequency resonant inverter topology with low voltage stress. *Paper presented at the IEEE Power Electronics Specialists Conference, Vols 1-6*, 2705-2717.

Rivas, J. M., Han, Y. H., Leitermann, O., Sagneri, A. D., & Perreault, D. J. (2008). A high-frequency resonant inverter topology with low-voltage stress. *IEEE Transactions on Power Electronics, 23*(4), 1759-1771.

Sallan, J., Villa, J. L., Llombart, A., & Sanz, J. F. (2009). Optimal Design of ICPT Systems Applied to Electric Vehicle Battery Charge. *IEEE Transactions on Industrial Electronics, 56*(6), 2140-2149.

Sallán, J., Villa, J. L., Llombart, A., & Sanz, J. F. (2009). Optimal design of ICPT systems applied to electric vehicle battery charge. *IEEE Transactions on Industrial Electronics, 56*(6), 2140-2149.

Sokal, N. O., & Sokal, A. D. (1975). Class E-A new class of high-efficiency tuned single-ended switching power amplifiers. *IEEE Journal of Solid-State Circuits, 10*(3), 168-176.

Takanashi, H., Sato, Y., Kaneko, Y., Abe, S., & Yasuda, T. (2012). A Large Air Gap 3 kW Wireless Power Transfer System for Electric Vehicles. *Paper presented at the IEEE Energy Conversion Congress and Exposition*, 269-274.

Tie, S. F., & Tan, C. W. (2013). A review of energy sources and energy management system in electric vehicles. *Renewable and Sustainable Energy Reviews, 20*, 82-102.

Wu, H. H., Gilchrist, A., Sealy, K. D., & Bronson, D. (2012). A High Efficiency 5 kW Inductive Charger for EVs Using Dual Side Control. *IEEE Transactions on Industrial Informatics, 8*(3), 585-595.

Yusmarnita Yusop, S. S., Sing Kiong Nguang, Huzaimah Husin, and Zamre Ghani. (2016). Design of Capacitive Power Transfer Using a Class-E Resonant Inverter. *JPE, 16*(5), 1678-1688.

Zhang, H., Lu, F., Hofmann, H., Liu, W., & Mi, C. C. (2016). A Four-Plate Compact Capacitive Coupler Design and LCL-Compensated Topology for Capacitive Power Transfer in Electric Vehicle Charging Application. *IEEE Transactions on Power Electronics, 31*(12), 8541-8551.

Zhang, W., & Mi, C. (2015). Compensation Topologies for High Power Wireless Power Transfer Systems. *IEEE Transactions on Vehicular Technology, PP*(99), 1-1.

Zhang, W., Wong, S. C., Tse, C. K., & Chen, Q. H. (2013). Analysis and Comparison of Secondary Series- and Parallel-Compensated IPT Systems. *Paper presented at the 2013 Ieee Energy Conversion Congress and Exposition*.

Zhang, W., Wong, S. C., Tse, C. K., & Chen, Q. H. (2014). Analysis and Comparison of Secondary Series- and Parallel-Compensated Inductive Power Transfer Systems Operating for Optimal Efficiency and Load-Independent Voltage-Transfer Ratio. *IEEE Transactions on Power Electronics, 29*(6), 2979-2990.

LIST OF PUBLICATIONS AND PAPERS PRESENTED

Journal

1. **Mohammad Kamar Uddin**, Saad Mekhilef and Gobbi Ramasamy. "Compact wireless IPT system using a modified voltage-fed multi-resonant class EF_2 inverter". Journal of Power Electronics (Accepted for publication, ISI-Cited Publication, I.F.: **1.047**, Q3).

Conferences

1. Uddin, M. K., Kalwar, K. A., Mekhilef, S., & Ramasamy, G. (2015, 5-6 June 2015). A wireless vehicle charging system using Class Φ2 inverter. Paper presented at **the Emerging Technologies: Wireless Power (WoW), 2015 IEEE PELS Workshop on.**
2. M. Kamar Uddin, G. Ramasamy, S. Mekhilef, K. Ramar, and L. Yew-Choy, "A review on high frequency resonant inverter technologies for wireless power transfer using magnetic resonance coupling," in ***2014 IEEE Conference on Energy Conversion (CENCON)***, 2014, pp. 412-417.
3. K. Kalwar, Mekhilef, S., Aamir, M., Uddin, Mohammad Kamar, "A New Coil Design for Enhancement in Misalignment Tolerance of Wireless Charging System", 13th IEEE SCORED, December 2015.